SELECTIVE DNA DEHYBRIDIZATION INDUCED BY LASER IRRADIATION ON GOLD NANOSTRUCTURES

by

Zhifeng Jiang
B.Sc., Peking University, 2006

THESIS SUBMITTED IN PARTIAL FULFILLMENT OF
THE REQUIREMENTS FOR THE DEGREE OF

MASTER OF SCIENCE

In the
Department of Chemistry

SIMON FRASER UNIVERSITY

Summer 2010

APPROVAL

Name: **Zhifeng Jiang**

Degree: **Master of Science**

Title of Thesis: **Selective DNA Dehybridization Induced by Laser Irradiation on Gold Nanostructures**

Examining Committee:

Chair: **Dr. Michael Eikerling**
Associate Professor, Department of Chemistry

_____

Dr. Hua-Zhong Yu
Senior Supervisor
Professor, Department of Chemistry

_____

Dr. George R. Agnes
Supervisor
Professor, Department of Chemistry

Dr. David Vocadlo
Supervisor
Associate Professor, Canada Research Chair,
Department of Chemistry

_____

Dr. Nancy Forde
Internal Examiner
Assistant Professor, Department of Physics

Date Defended/Approved: August 11, 2010

Declaration of
Partial Copyright Licence

ABSTRACT

The objective of this thesis is to explore the feasibility of using light to control the surface reactions of DNA-Au nanoconjugates. Two types of gold nanostructures (Au nanoparticles vs. Au/SiO_2 nanoshells) were modified with DNA oligonucleotides with different sequences. Due to the variation of their surface plasmon resonance peaks (520 nm for nanoparticles, 1100 nm for nanoshells), laser beams with corresponding wavelengths were used to irradiate the mix samples. It has been demonstrated that the laser-induced (photo-thermal effect) dehybridization of the dsDNAs on these nanostructures is selective, i.e., we can either release the single strands from the nanoparticles or from the nanoshells in the same solution independently. The experimental conditions have been optimized based on the selection of irradiation time and laser power. The selective, “remote” control of DNA reactions on the surface of nanostructures has potential applications in various clinical areas such as drug delivery and *in vivo* diagnostics.

Keywords: biosensor; DNA; selective dehybridization; gold nanostructure; laser; surface plasmon resonance.

ACKNOWLEDGEMENTS

I would like to sincerely thank my senior supervisor, Dr. Hua-Zhong (Hogan) Yu for giving me the opportunity to carry out this research in his lab. I thank him for his guidance, advice, encouragement and patience throughout my studies at SFU.

I would like to thank Dr. Hidehiko Asanuma for his great help throughout my research. Dr. Bixia Ge for training me in my early stages of my project and turning me into a scientific researcher, Dr. Yunchao Li for his generous help with his profound and extensive knowledge, Dr. Banani Chakraborty for all the discussions and helpful ideas. I thank Dr. Eberhard Kiehlmann for great help in editing the thesis.

I would like to thank my committee members, Dr. David Vocadlo and Dr. George Agnes for discussions and helpful suggestions. I thank all the past and present members of the Yu-Lab (Alan, Davin, Dinah, HongLun, Joe, Lily, Marcus, Navanita, Richard, Weiguo) for their friendship and making my stay at SFU worthwhile. I am also grateful for Dr. Kohei Uosaki, Dr. Katsuyoshi Ikeda and all the members of Uosaki-Lab for their help and kindness during my study at Hokkaido University in Sapporo, Japan.

Last but definitely not the least I thank my parents for their support and encouragement.

TABLE OF CONTENTS

LIST OF FIGURES

LIST OF TABLES

GLOSSARY

APTES (3-aminopropyl) triethoxysilane

AuNP gold nanoparticle

AuNS gold nanoshell

b.c.c. body-centered-cubic

BSA bovine serum albumin

CS_2 carbon disulfide

CTAB cetyltrimethylammonium bromide

Cy5 Indodicarbocyanine

dsDNA double stranded DNA

DTT dithiothreitol

FAM carboxyfluorescein

f.c.c. face-centered-cubic

FL fluorescence

$HAuCl_4$ tetrachloroauric (III) acid

LCST lower critical solution temperature

MEMS micro-electromechanical systems

$NaBH_4$ sodium borohydride

NHS *N*-hydroxysuccinimide

NIR near infrared

PBS phosphate buffered saline

RFMF radio-frequency magnetic field

SAM self-assembled monolayer

SDS sodium dodecyl sulfate

SHG second-harmonic generator

SPR surface plasmon resonance

ssDNA single stranded DNA

TAMRA tetramethylrhodamine

TCEP tris (2-carboxyethyl) phosphine hydrochloride

TEM transmission electron microscopy

1: INTRODUCTION

1.1 Gold nanostructures in history

History of gold nanostructures goes back to the 4th millennium B.C. in Egypt, China and later Europe. Gold colloids, typically 5-60 nm in size, were used to make ruby glass and colored ceramics[1, 2]. A famous example is the Lycurgus Cup made in the 4th century B.C. in Rome, showing King Lycurgus being dragged into the underworld by a vine. In reflected light, for example in daylight, it appears green. However, in transmitted light, i.e., when light is shone from inside the cup, it shows a ruby red color[3] (Fig. 1.1).

Figure 1.1 Lycurgus Cup. It appears green in daylight (left). In transmitted light it shows a ruby red color (right). Adapted from reference 3.

Applications of gold colloids in glass and ceramics continued afterwards: “drinkable gold” was believed to cure various diseases in the Middle Ages. Many scientists and doctors did research on gold colloids for their value in medicine, and they began to understand the relation between gold colloid size and its color: “Pink or purple solutions contain gold in the finest degree of subdivision, whereas yellow solutions are found when the fine particles have aggregated”[2, 4]. In 1857, Faraday published his well-known work “Bakerian Lecture: Experimental Relations of Gold (and Other Metals) to Light”, in which he did not only describe the preparation of the first pure sample of colloidal gold from chloroaurate and phosphorus, but also its properties in solution and on film[5].

Au nanostructures have gained a great deal of interest and have been intensively investigated in the past two decades. Numerous research articles, reviews and books[2, 6-10] have been published, describing colloidal gold a widely used material in diagnostics, therapeutics, catalysis, optical sensing, and other areas in nanotechnology. In the following section, several examples of gold nanostructure applications are given.

1.2 Gold nanostructures: from sphere and rod to core-shell

Au nanoparticles (AuNPs), usually in the form of colloidal gold, have a typical diameter between 1 and 100 nm. As synthesized by Faraday and many others, they are usually suspended in water. The liquid has usually either an intense red color (for particles less than 100 nm), or a dirty yellowish color (for larger particles). Spherical AuNPs are the most common, while other shapes, like rod, shell, cube, and cap, can also be synthesized in certain procedures.

Generally, spherical AuNPs are synthesized by reduction of tetrachloroauric acid ($HAuCl_4$) in solution. Faraday used phosphorus as reducing agent in a binary carbon disulfide (CS_2)-water mixture. Nowadays, sodium citrate is used as the most popular reducing agent toward $HAuCl_4$, which was introduced by Turkevitch in 1951[11]. It produces suspended spherical AuNPs of around 10-20 nm diameter. Larger particles can also be made, but monodispersity and shape are compromised. The citrate ions first act as reducing agent, and later can be absorbed onto the surface of the particles as stabilizing agent, making the particles negatively charged, preventing aggregation by mutual repulsion. The most updated synthesis protocol is as following[12]: the reduction is initiated by bringing a $HAuCl_4$ solution to boiling in a double-walled reactor, which assures a very homogeneous temperature distribution within the solution. When the solution starts to boil, a preheated citrate solution can be added. The citrate concentration can be varied to achieve different particle sizes[13]. After a defined time (normally 15 minutes), the liquid is then extracted and cooled to room temperature[12]. The solution is typically kept boiling for normally 1 hour to reach the desired AuNP size. The overall reaction can be described as follows[11]:

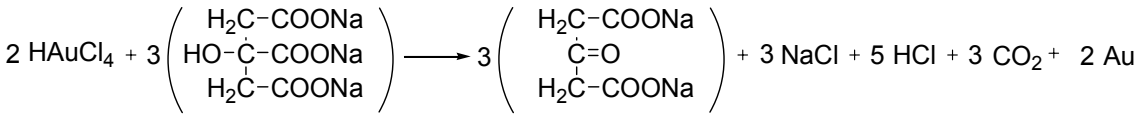

The key experimental facts are 1) $HAuCl_4$ is completely converted to $Au_{(s)}$ in the presence of excess citrate[12]; 2) acetone dicarboxylic acid is identified as

the first intermediate product[11, 14]. Fig. 1.2 shows a typical transmission electron microscopy (TEM) image of thus prepared AuNPs with a diameter of 20±2 nm.

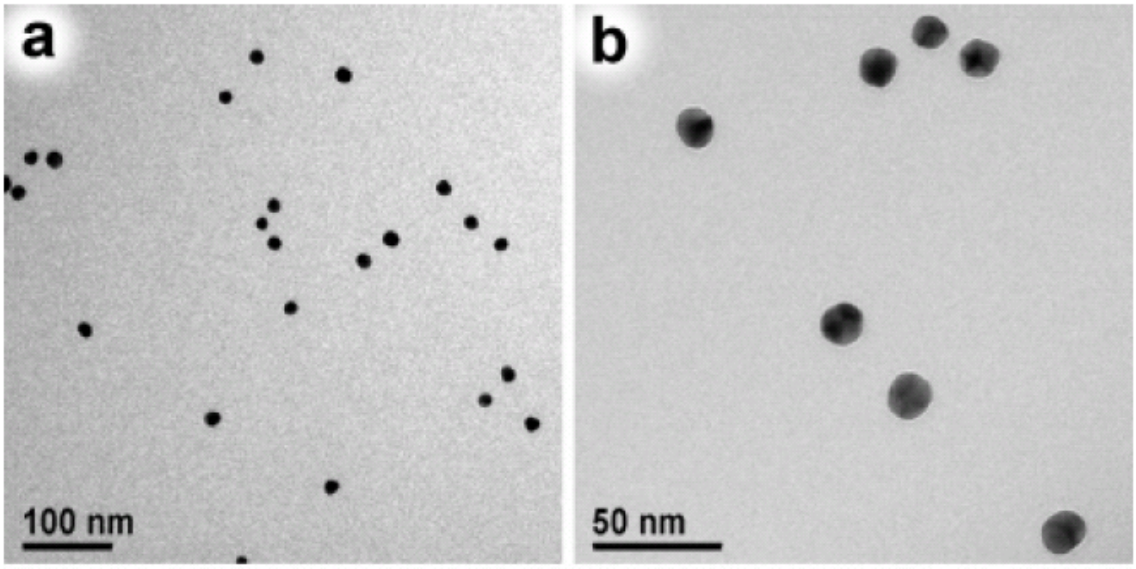

Figure 1.2 TEM images of AuNPs. Adapted from reference [15].

Optical properties of AuNPs are mostly dependent on their diameters[16-18]. Fig. 1.3 shows the Ultraviolet/Visible (UV/Vis) absorption spectra of AuNPs of different sizes in water. The maximum absorption red-shifts with increasing particle diameter (λ_{max} = 517, 521, 533, and 575 nm for the 9-, 22-, 48-, and 99-nm particles, respectively). With the increasing of the particle size, it was also noticeable that the peak width first decreases, followed by an increase, with a minimum for the 22-nm nanoparticles.

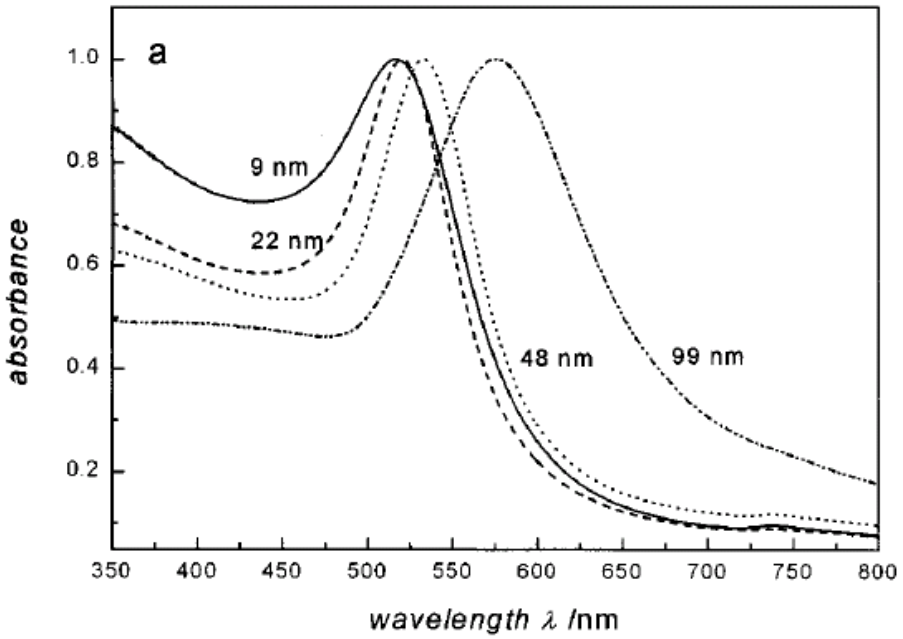

Figure 1.3 UV/Vis absorption spectra of 9, 22, 48, and 99 nm AuNPs in water. All spectra are normalized at their absorption maxima, which are 517, 521, 533, and 575 nm, respectively. Adapted from reference 16.

Mie theory has been proposed to estimate the maximum extinction wavelength quantitatively by solving Maxwell's equations with the appropriate boundary conditions for spherical particles[19]. Particularly for nanoparticles that are small compared to the wavelength of the exciting light (for AuNP diameter < 25 nm) only the dipole absorption of the Mie equation contributes to the extinction of the nanoparticles. For larger nanoparticles (diameter > 25 nm) the extinction is also dependent on quadrupole and octopole absorptions[20]. These higher modes explicitly depend on the particle size, therefore with increasing size the optical absorption maximum is shifted to longer wavelength[16].

Haiss et al. pioneered the study of the size dependence of AuNPs[18]. Several types of AuNPs with diameters ranging from 5 to110 nm were

synthesized in their work. The maximum absorbance peak position is plotted as function of diameter (Fig. 1.4). All the calculated data (based on Mie theory) and experimental data are plotted on the same graph. It can be seen that theoretical and experimental data are generally in agreement, especially when particle size is larger than 25 nm. For sizes larger than 25 nm, Haiss et al were able to fit the peak positions precisely to a simple exponential function (R^2 = 0.99):

$$\lambda_p = \lambda_o + L_1 \exp(L_2 d) \quad (1)$$

where λ_p is the experimental peak position, d is the particle diameter. The fitting parameters are λ_o = 512 nm, L_1 = 6.53 nm, L_2 =0.0216 nm^{-1}. This equation is particularly helpful to determine AuNP size based on its peak absorbance.

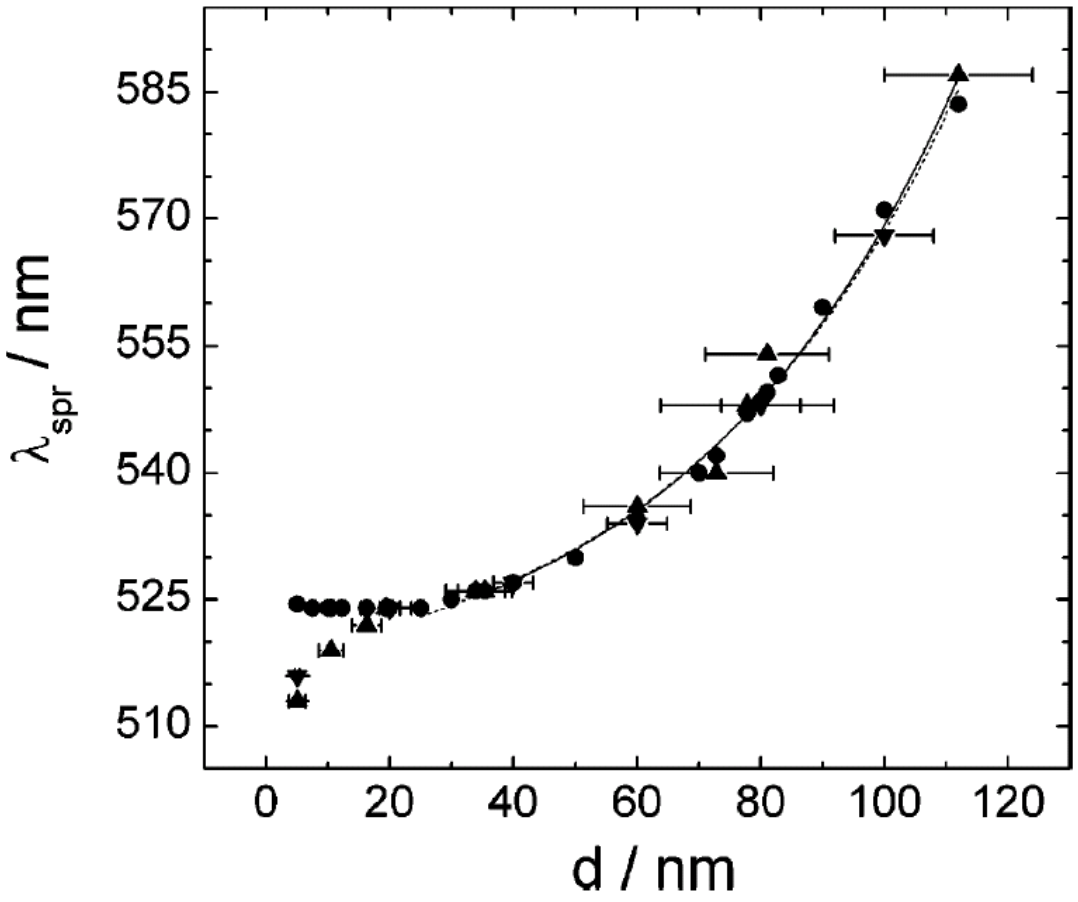

Figure 1.4 Position of the absorbance peak (or surface plasmon resonance peak, λ_{spr}) as a function of the particle diameter for AuNPs in water: calculated (circles); experimentally measured (downward-pointing triangles, commercial Au nanoparticles; upward-pointing triangles, in-house synthesized Au nanoparticles). An exponential fit to the theoretical (experimental) data for d > 25 nm is shown as a solid (dashed) line. Adapted from reference 18.

A nanorod is a type of nanostructure with a particular morphology, i.e., the typical aspect ratio (length divided by width) is from 3 to 5. Its typical dimension range is from 1-100 nm. Nanorods are usually produced by a seeding-growth procedure. Spherical Au nanoparticle seeds (~ 4 nm) are produced by a fast and complete reduction of $HAuCl_4$ with a strong reducing agent like sodium borohydride ($NaBH_4$):

$$8AuCl_4^- + 3BH_4^- + 9H_2O \rightarrow 8Au_{(s)} + 32Cl^- + 3H_3BO_3 + 21H^+$$

The excess amount of $NaBH_4$ assures that no $HAuCl_4$ is left to grow into large AuNP. Then the seeds are added to a growth solution, which contains $HAuCl_4$, cetyltrimethylammonium bromide (CTAB) as a surfactant and ascorbic acid as a weak reducing reagent. The presence of these reagents causes the seeds to grow into Au nanorods instead of AuNPs. The shape and aspect ratio of a nanorod can be controlled by the concentration of each reagent and the reaction time[21, 22]. Physical and chemical properties of Au nanorods are diverse but can be tuned by changing the size and aspect ratio (Fig. 1.5). For example, absorbance peak shifts from ~800 nm to ~1100 nm when aspect ratio increases

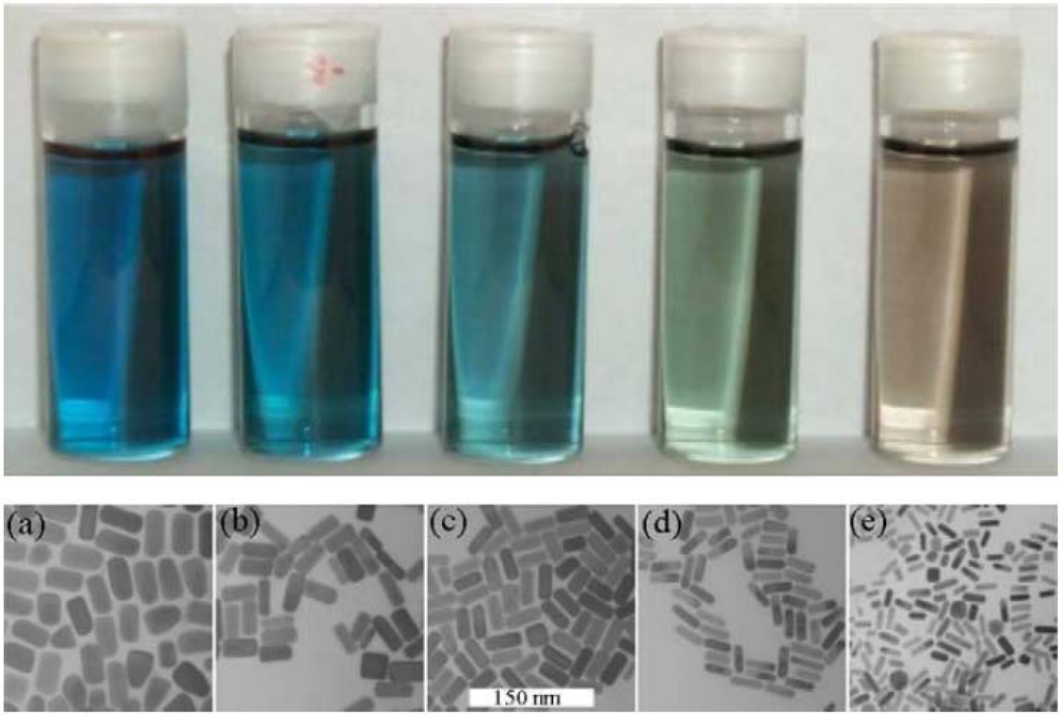

Figure 1.5 The color of gold nanorods and the respective micrographs. The color changes take place for very small changes in mean aspect ratio. Adapted from reference 8.

from 4.0 to 5.4 (mainly due to the decrease in its width)[22].

Au nanoshells (AuNSs) are characterized by their tunable extinction spectra. A metal nanoshell consists of a spherical dielectric nanoparticle surrounded by an ultrathin, conductive, metallic layer[23-25] (Fig. 1.6). By varying the composition and dimension of the layers of the nanostructures, nanoshells can be designed and fabricated with maximum extinction from UV to infrared regions of the spectrum[26] (red-shifted from AuNP, due to change in size and composition). They can thus be specifically designed to match the wavelength required for a specific application. In particular, AuNSs are usually synthesized from a silica core and a thin gold layer as shell[24]. The AuNS extinction peak reaches the near infrared (NIR) region where light penetrates blood and tissue. In comparison, extinction peak of conventional gold nanoparticles is located in the visible region, where light is absorbed by blood and tissue. This makes AuNS valuable in cancer therapy and other medical research areas[27], for example, in biomolecular optical imaging of cancer cells and tissue[28]. An AuNS monolayer has been made to monitor the concentration of streptavidin in 20% whole blood[29]. Prior to reference 29, spectrometric analysis of conventional whole-blood samples has been rarely carried out, because the complex biology and the high absorption intensity of whole blood often strongly interfere with the optical signal. AuNSs are thus introduced in reference 29 to shift the spectrum into the NIR region in order to minimize background interference. As shown in Fig. 1.7, AuNSs are deposited on a glass substrate modified with an (3-aminopropyl) triethoxysilane (APTES) self-assembled monolayer (SAM). Biotin-*N*-

Hydroxysuccinimide (Biotin-NHS) is then immobilized onto the SAM via bridge formed from cystamine. This glass chip is then immersed in a bovine serum albumin (BSA) solution for 5 hours to block the empty sites, i.e., to eliminate direct contact between AuNS and the whole blood sample. When the streptavidin is present in the sample, it is captured by the biotin localized on the surface. This causes a change of the surrounding refractive index, transducing this biomolecular binding event into an optical signal[17, 30-33]. As a result, increased absorbance of the gold nanoshell is successfully detected by NIR spectrophotometry.

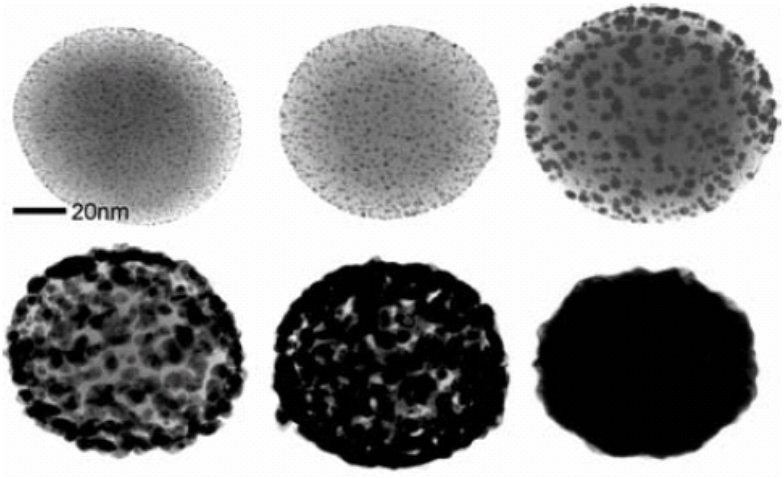

Figure 1.6 Series of TEM images showing gold colloids' growth into a complete shell on silica core particle surface. Beginning from the upper left, the gold colloids (dark dots) serve as nucleation sites for additional electrodeless plating of gold. As additional gold is deposited onto the gold islands, the gold grows until coalescing with neighboring colloids, finally forming a complete metal shell (bottom right). Adapted from reference 25.

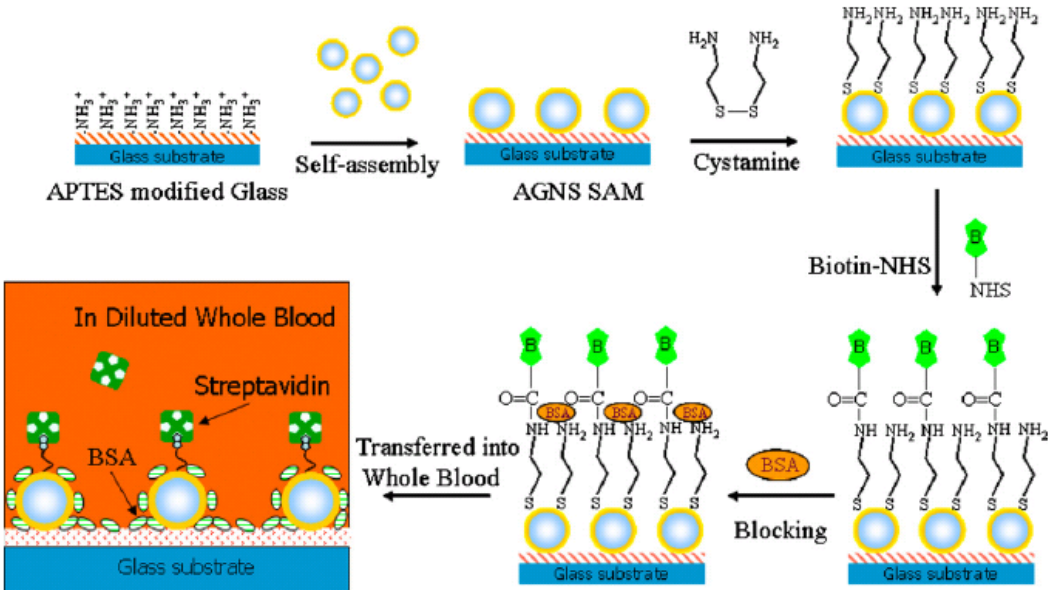

Figure 1.7 Schematic fabrication process of the gold nanoshell SAMs and the analysis of streptavidin. Adapted from reference 29.

1.3 Manipulation of surface reactions on DNA-Au nanoconjugates

The concept of coupling Au nanostructures with DNA was introduced in the 1990s[7, 34-37]. Merging of these two distinctive areas creates some interesting properties and functionalities, including one-, two- and three-dimensional nanostructures, molecular capture and release, surface plasmon resonance heating, etc. Fig. 1.8 shows a general scheme of coupling AuNP with DNA, which includes immobilization, salt aging and wash. Adding electrolyte (salt aging) helps immobilization by neutralizing the negative charge of DNA and AuNP thus minimizing electrostatic repulsion. DNA can be completely removed from AuNP by adding DTT, which cleaves the gold-thiol bond.

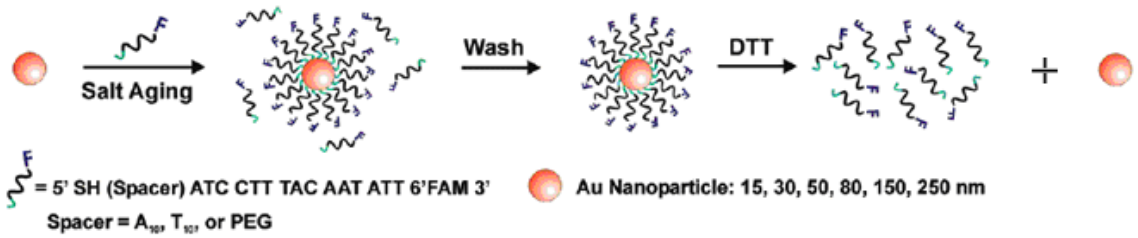

Figure 1.8 Synthesis of DNA-modified AuNP. F represents fluorophore. Adapted from reference 38.

Mirkin's group at Northwestern University is one of the leading teams in the DNA-Au nanostructure related area. One of their recent publications shows programmable nanoparticle crystallization controlled by DNA[39]. It is demonstrated that DNA linkers can guide Au nanostructures into crystallization, in which the same type of Au nanoparticles leads to different crystalline states by using different DNA sequences. As shown in Fig. 1.9, when all Au nanoparticles are modified with one type of DNA (linker A), a single-component system is obtained in which the Au nanoparticles form a face-centered-cubic (f.c.c.) crystal structure. In this system the linker DNA is self-complementary. When linker X and linker Y were immobilized on Au nanoparticles, a binary system is established in which X is conjugated with Y, but not with another X. This results into a body-centered-cubic (b.c.c.) crystal structure, where one Au nanoparticle is surrounded only by its counter species. As a result, the crystal structure becomes entirely different, although the distance between two nearest Au nanoparticles stay relatively unchanged. Since the assembled structure contains only 3% inorganic material by volume, it is measured by small-angle X-ray scattering. In a subsequent research, it is shown that lattice constants can be adjusted by using DNA linkers of different lengths[40].

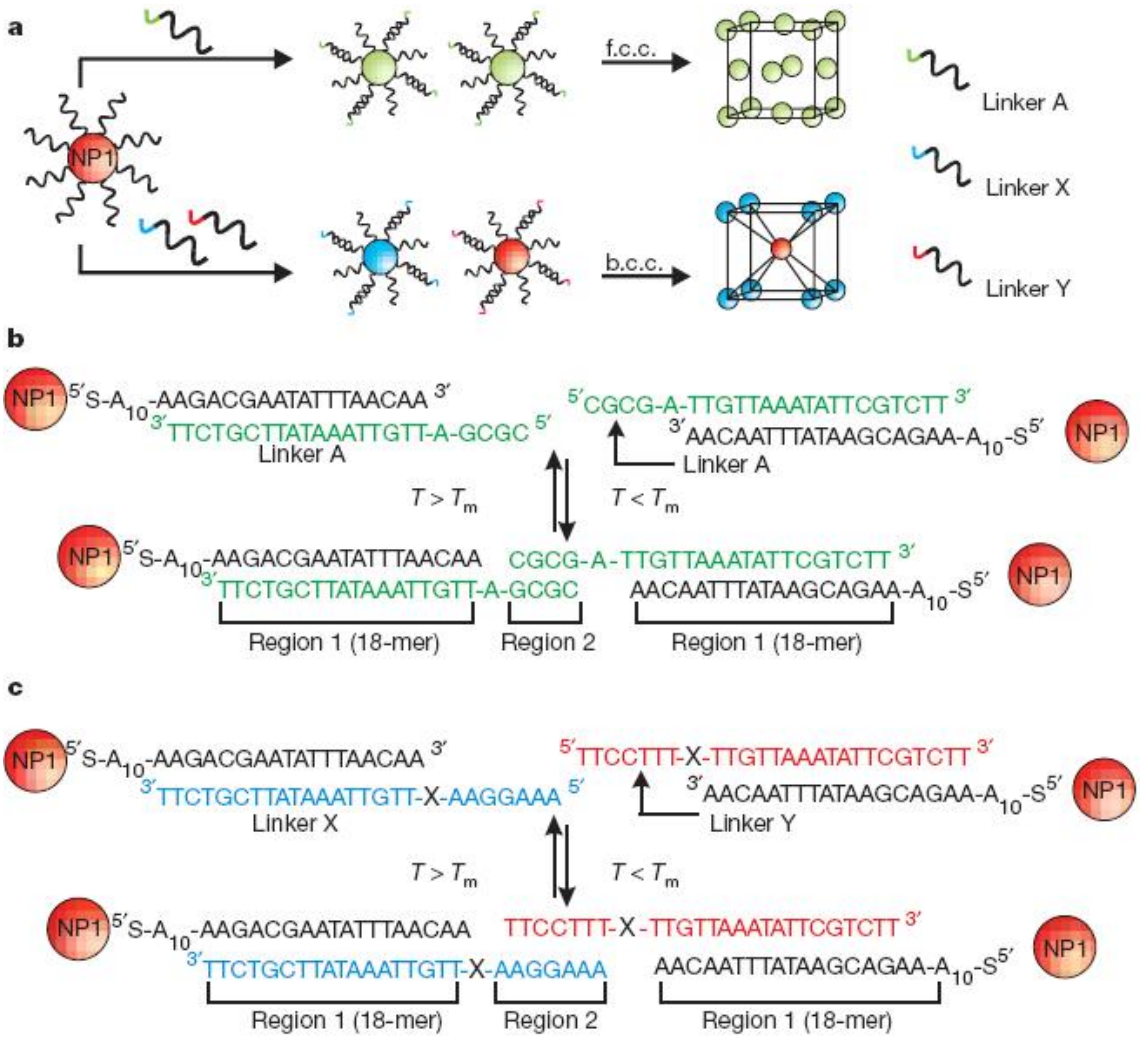

Figure 1.9 (a) DNA-Au nanoparticle conjugates have been designed to assemble into single-component or binary crystal structures by changing the sequence of the DNA linkers. (b) Single-component assembly leads to f.c.c. crystallization by linker A. (c) Binary-component assembly leads to b.c.c. crystallization by linkers X and Y. Adapted from reference 39.

Au nanostructures have been extensively used as fluorescence (FL) quenchers in recent years[10, 41-45]. The advantages of Au nanostructure quenchers compared with traditional organic dyes are mainly efficiency[46] and photostability[47]. When an Au nanostructure is utilized as a FL quencher, two opposite phenomena can be observed depending on the fluorophore-quencher

distance. When the distance between fluorophores and metallic surfaces is smaller than 5 nm, strong quenching of FL emission and a dramatic reduction of the excited states lifetimes is observed[48-51]. When this distance is in the range of 10-20 nm, enhanced FL emission can be achieved because of local concentration of the incident excitation field by the metallic nanostructures[52-54]. This enhancement highly depends on their distance and decays rapidly as their distance exceeds 20 nm. A recent paper[45] has described the labeling of monoclonal 2F5 anti-biotin antibody with fluorophore Alexa 488, while the Au nanoparticles (core diameter of 20 nm) were biotinylated. The “Y”-shaped molecules represent the anti-biotin antibodies, the short “I” rods represent the biotin groups, and the black ring represents the nanoparticle (Fig. 1.10). The initial solution contains 4.30 nM free anti-biotin, which gives a relatively high FL intensity. When a 0.86-nM solution of biotinylated Au nanoparticles is introduced at 60 seconds, the FL intensity decreases significantly. This could be due to three combined effects: 1) dilution by the nanoparticle solution; 2) absorption and scattering caused by the presence of nanoparticles; and 3) actual quenching of the emission intensity by the gold nanoparticles as the antibody binds to biotin groups anchored on the nanoparticles. In order to separate the quenching effect from the rest, a control experiment has been carried out in which a blocked anti-biotin was used instead of active anti-biotin. The blocked anti-biotin wouldn’t interact with biotin. Comparison clearly demonstrated that a significant FL intensity decrease is caused by quenching. Introduction of free biotin in solution

(1 mM) afterwards results in the recovery of FL emission. Au nanostructures could be considered as good alternative quenchers in FL-based applications.

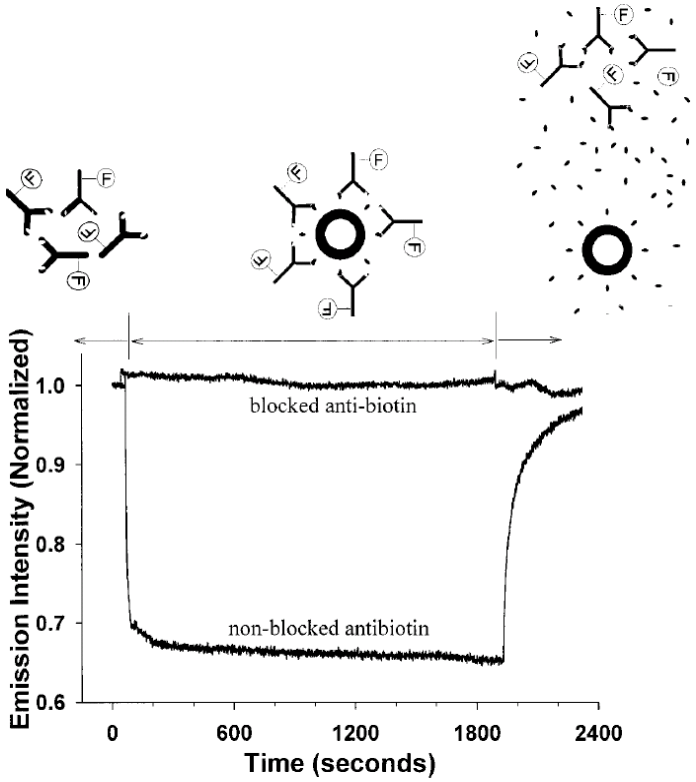

Figure 1.10 FL emission intensity (normalized) of Alexa 488-labeled anti-biotin antibodies interacting with biotinylated gold nanoparticles. Adapted from reference 45.

1.4 Surface plasmon resonance of gold nanostructure

All the three aforementioned Au nanostructures are capable of generating surface plasmon resonance (SPR). Free electrons in a metal may be considered as an electron plasma state. When the frequency of an incident electromagnetic wave (e.g. light) overlaps with the oscillating frequency of electrons in the AuNP, the electric field induces a “dipole”, which can be described as a small, uniform

displacement of the electric cloud to cancel the internal electric field (Fig. 1.11). This causes a repeated movement of electrons, and forms a collective oscillation of electrons on the surface of the particle. This collective oscillation of electrons in the presence of light is called SPR[55]. Both metal and dielectric are essential in the formation of SPR, which reaches its maximum in the metal-dielectric interface and decays into both media, in the direction perpendicular to the interface[56].

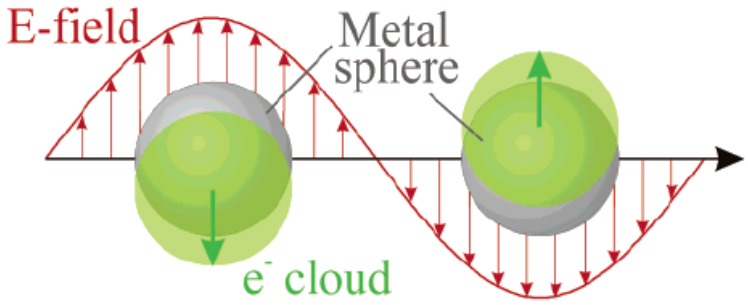

Figure 1.11 Schematic of plasmon oscillation for a sphere, showing the displacement of the conduction electron charge cloud relative to the nuclei. Adapted from reference 20.

The SPR of Au nanostructures occurs over a wide frequency range which depends on the dielectric and geometry of the colloids. The SPR absorption of Au nanostructures follows Beer's law, which states that the absorption is dependent on concentration, extinction coefficient and the path length of a sample[57].

When Au nanostructures are irradiated with light corresponding to their SPR frequency, the energy is absorbed and transformed to heat through a series of cascading events[58, 59]. Firstly, due to mutual repulsion, a strong electron-electron scattering would occur and lead to a rapid dephasing of the electronic coherent oscillation (in ~500 femtoseconds)[60]This generates a pulse of hot

electrons of tens of thousands of degrees. These hot electrons relax by collision with lattice ions, resulting in heating the gold nanocrystal lattice via electron-phonon interaction, which occurs in ~1 picosecond[61]. The lattice cools by giving its heat to the surrounding medium via phonon-phonon relaxation in ~100 picoseconds[61, 62]. This photothermal effect makes it possible to turn an Au nanostructure into a nanoscale “stove” to heat the molecules attached as well as the local environment[59].

Research of Au nanostructure SPR heating effect was begun in the 1990s[24, 63-65]. Villringer et al. reported non-invasive optical spectroscopy and imaging of human brain function at the time, and pointed out potential clinical treatment by light in 800-1200 nm range[64]. Au nanostructures, especially AuNSs, then drew scientists’ attention for their tunable SPR bands in this NIR range. At the World Biomaterials Congress 2000, Halas and West reported an important finding for hydrogel polymers[66]. The hydrogel they used had a lower critical solution temperature (LCST) slightly above body temperature. It collapses when the temperature rises above this value. AuNSs are incorporated into this hydrogel so that NIR light can be converted to heat, causing hydrogel deswelling (Fig. 1.12). Originally, soluble medicine is proposed to be held within the hydrogel matrix, thus stabilized and protected. When the hydrogel is delivered to the designated region in the human body and that region is irradiated with an NIR laser, the light penetrates, eventually reaches the hydrogel and heats the AuNSs, leading to hydrogel collapse and deswelling, thus releasing the corresponding medicine.

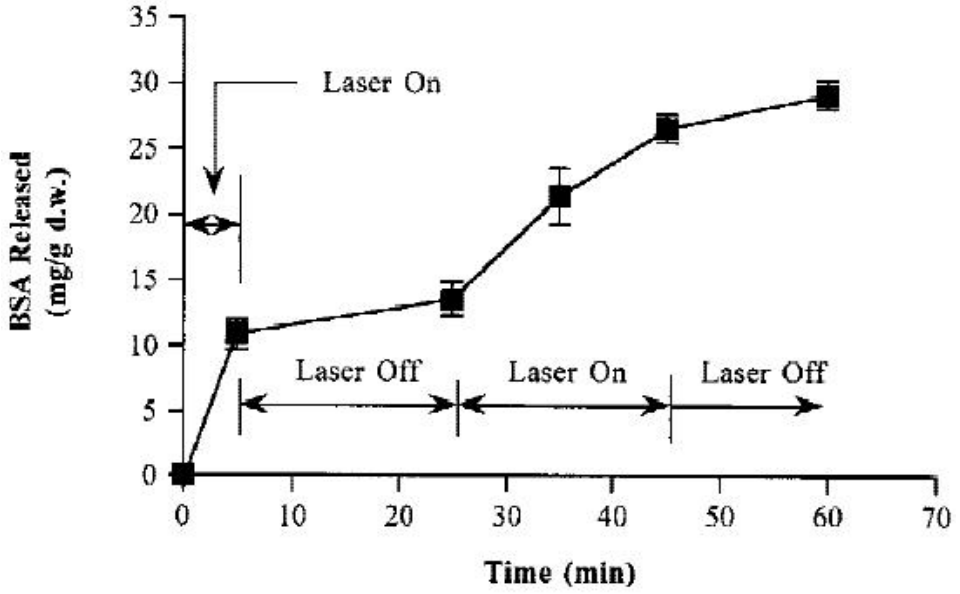

Figure 1.12 Release of BSA from nanoshell-composite hydrogels in response to sequential irradiation at 1064 nm (164 mJ/pulse, 7-ns pulse length, 10-Hz repetition rate) during the 0-5 minutes and the 25-35 minutes period. Adapted from reference 66.

Halas and West's research was followed by other chemists, who did not only use hydrogel[67, 68], but also DNA as responding material for Au nanostructure SPR heating[22, 69-74]. In a related research, a radio-frequency magnetic field (RFMF) was applied to excite the Au nanoparticle in order to generate heat[69]. A 1.4 nm-diameter gold nanoparticle is covalently linked to the centre of a DNA oligonucleotide. The DNA is designed to be partially complementary to itself with 7 base pairs forming a hairpin-loop structure in its stable state (Fig. 1.13a). The RFMF parameters are calculated and designed to make the generated heating depth larger than the particle diameter, so the entire particle can be heated. When the magnetic field is turned on, the Au nanoparticle is excited and heated, dissociating the DNA base pairs and dissembling the hairpin structure. This base

pair dissociation could be monitored by change in optical absorbance at 260 nm, due to the hyperchromicity phenomenon when a DNA duplex is denatured[75, 76]. Because of the loop constraint, the DNA rehybridizes on a timescale comparable to dehybridization when the magnetic field was turned off[77] (Fig. 1.13b).

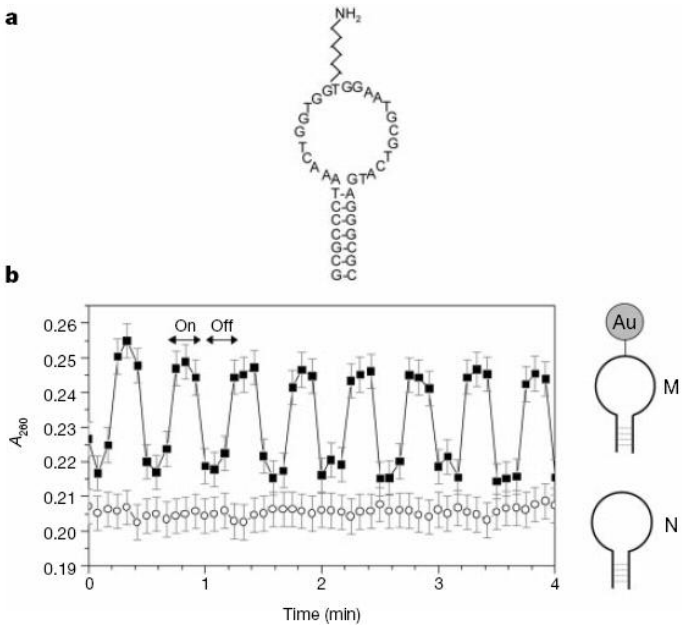

Figure 1.13 (a) Sequence of the hairpin DNA (M). The DNA sequence is self-complementary at the ends for 7 bases. (b) Absorbance at 260 nm of a solution of M in RFMF (squares). Arrows indicate when the RFMF is on/off. Circles represent the response of the same DNA without attached Au nanoparticle (N). Adapted from reference 69.

Laser light, due to its high power density, is considered a superior candidate to remotely excite Au nanostructures and generate a localized heating effect. Stehr et al. have used a 300-ns laser to dehybridize DNA oligonucleotides attached to Au nanoparticles[73]. The target molecule of this research was a 30-base single stranded DNA (ssDNA) sequence with no modification (in green in Fig. 1.14a). Two different types of ssDNA sequences are immobilized on Au

nanoparticles of 10 nm diameter (in blue and red in Fig. 1.14a). Each ssDNA sequence consists of a thiolated A_{15} sequence as spacer and 15 further bases as detection sequence. The two detection sequences of 15 bases are complementary to the two ends of the 30 bases of the target ssDNA, respectively. Hybridization of these three ssDNA sequences brings the Au nanoparticles together to form a large nanoparticle aggregate (Fig.1.14b). When this aggregate is irradiated by laser, the Au nanoparticles absorb photon energy and then generate heat, which dehybridizes and melts the DNA linkers, causing Au nanoparticles to separate from each other. The detection method takes advantage of changes in the Au nanoparticle optical properties upon separation. When separated, the absorbance of dispersed Au nanoparticles is narrowed and blue-shifted (Fig. 1.14c). A pump laser is positioned at 527 nm to irradiate, while a probe laser is positioned at 650 nm to monitor the decrease of Au nanoparticle extinction upon separation (Fig. 1.14c&e).

To release multiple DNA oligonucleotides selectively from Au nanostructures by SPR, Wijaya et al.[22] synthesized two types of nanorods with distinguished SPR bands (one called “nanocapsule” with aspect ratio of 4.0 and maximum SPR at 800 nm, the other called “nanobone” with aspect ratio of 5.4 and maximum SPR at 1000 nm). Two different DNA oligonucleotides were conjugated to these two types of the nanorods, respectively. When irradiated with laser at a specific wavelength, each nanorod melts into a nanoparticle thus cleaving the Au-S bonds and resulting in the detachment of the oligonucleotides from the surface. Since each DNA oligonucleotide is modified by a fluorophore

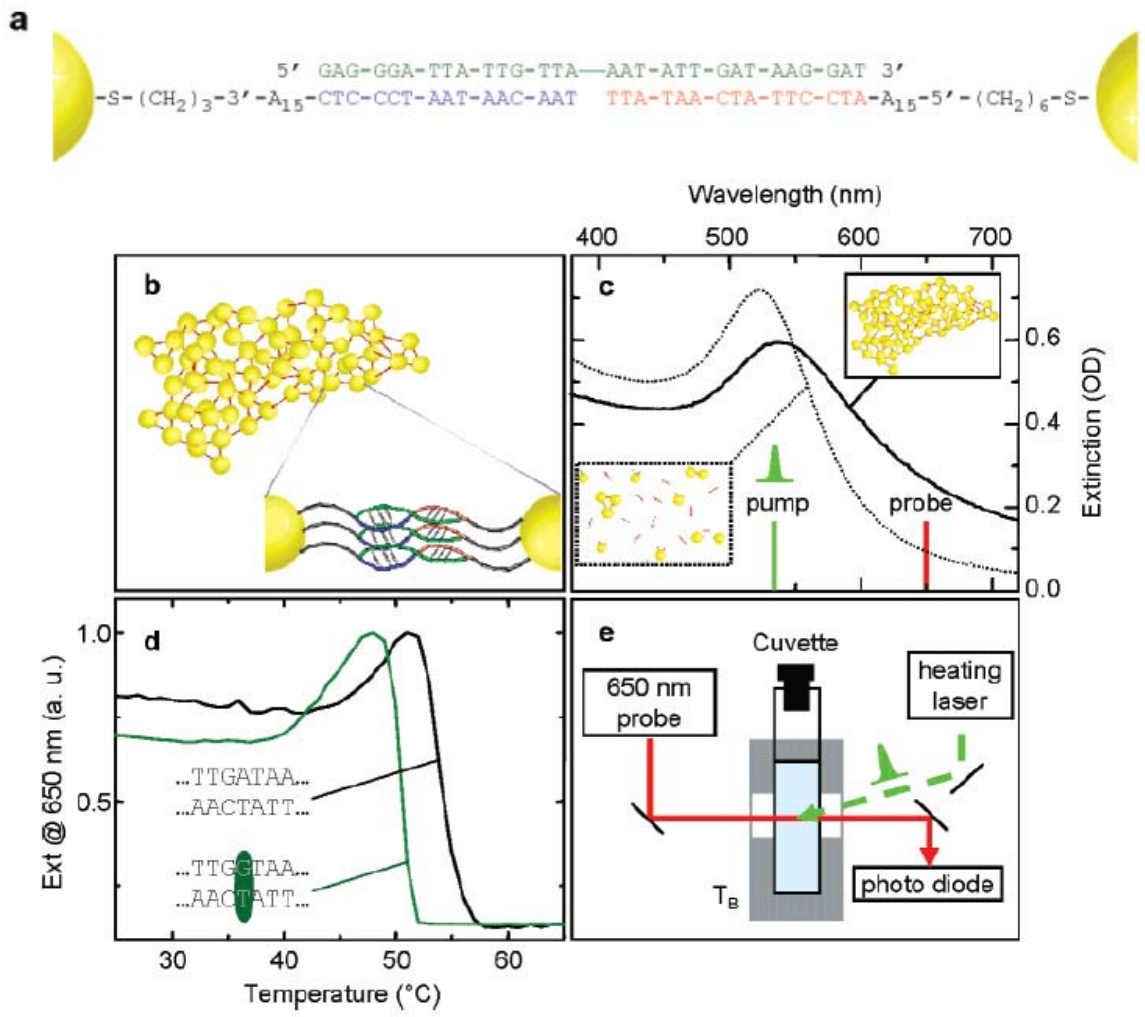

Figure 1.14 Gold nanostoves as DNA melting assay. (a) Two Au nanoparticles are linked by the sequences for a perfect matching target. (b) Diagram of Au nanoparticle aggregate and multiple inter-particle connections made by DNA hybridization. (c) Extinction spectrum of DNA-bound gold nanoparticle aggregates at 25 °C (solid line) and of dispersed particles at 60 °C (dotted line). The green line indicates the wavelength of the pump laser for heating and the red line shows the probe laser wavelength. (d) Extinction of the DNA-AuNP conjugates at 650 nm. The melting temperature of the dsDNA is 54.0 °C for the perfect matching target and 50.5 °C for a target with single base pair mismatch. (e) Experimental setup: the pulsed pump-laser (green) heats the gold aggregates. The corresponding change in the sample's extinction is monitored by a fast-response photodiode. Adapted from reference 73.

(carboxyfluorescein (FAM) for DNA on nanocapsule and tetramethylrhodamine (TAMRA) for DNA on nanobone), a FL spectrum is recorded for each DNA

dissociation event (Fig. 1.15). This is a novel method for multiple-drug delivery strategies, although the carrier (nanorod) is destructively (irreversibly) melted.

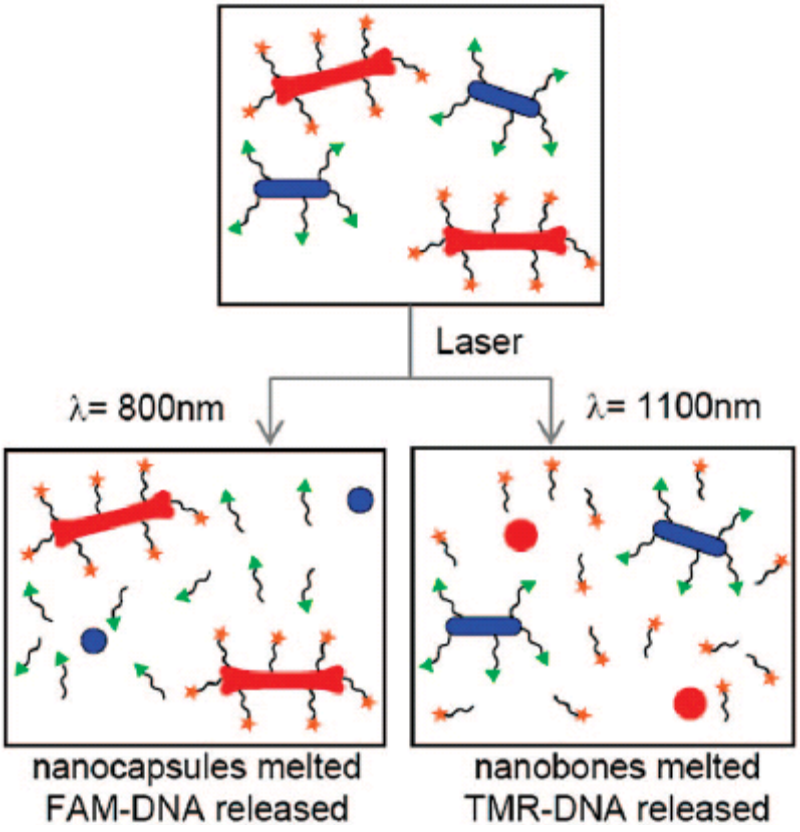

Figure 1.15 Laser irradiation of DNA-conjugated nanocapsules (blue ovals) and nanobones (red bones) at 800 nm (left) melts the nanocapsules and selectively releases the DNA (labelled by FAM (green triangles)). Irradiation at 1100 nm (right) melts the nanobones, selectively releasing the DNA (labelled by TAMRA (orange stars)). Adapted from reference 22.

All previously mentioned research takes advantage of the Au nanostructures' unique property of absorbing light at a certain wavelength and converting it to heat. On the other hand, because of rapid decay of SPR from interface to the dielectric, Au nanostructure only heats up a thin layer of water (~ 5 nm thick) in aqueous solution (calculated in detail in reference 78, also stated

in reference 73, 79). If the concentration is low and the distance between two nanostructures is large enough, each nanostructure only heats up its own surrounding area, instead of heating up the entire solution. Thus only the close environment of those particles is affected. This localized heating property of Au nanostructure has not yet been applied to DNA-related research.

What source can we use to only heat up a certain group of particles while leaving the rest unchanged? It has been shown that AuNSs have a tunable SPR band in the NIR range[66]. Different nanoshells respond to lasers of different wavelengths, which enable us to control their surrounding temperatures selectively in a mixed solution. This makes it possible to selectively heat a certain type of nanostructure, while leaving the rest unchanged. When a nanostructure is fabricated with DNA strands attached to it, it will only heat up and dehybridize DNAs attached to it, as the 5 nm thickness matches the length of a short DNA sequence. If several different sets of DNA are coupled to the nanoshells with different sizes, each nanoshell can be dehybridized depending on the wavelength of the laser irradiation.

1.5 Objective of this thesis

The objective of this thesis is to explore the feasibility of using light to control the surface reactions of DNA-Au nanoconjugates. We propose a design in which double stranded DNA (dsDNA) can be selectively dehybridized on Au nanostructures by laser stimulus at selected wavelength. Two dsDNA sequences will be prepared, for which one strand is modified with a thiol group for bonding to the Au nanostructure and the other strand is labeled with different fluorescent

tags. Due to the difference between their SPR peak wavelengths, the thermal effect of the nanostructures can be triggered at certain laser wavelengths thereby allowing selective dehybridization of the dsDNA of interest. Individual DNA-nanostructure dehybridization by laser has been explored before, but only towards single species. Wijaya's report is the only one that irradiated a mixed sample (two types of Au nanorods with two different dsDNAs immobilized)[22]. In their report, however, the high power output irreversibly removed (instead of dehybridized) DNA from the nanorod by melting the nanorod, in which case the nanorod structures were "destroyed".

2: EXPERIMENTAL

2.1 Reagents and materials

Two dsDNA sequences were constructed from four ssDNA sequences, named S1, S1', S2 and S2'. Two additional ssDNAs used in the adenosine-aptamer binding experiments were S3 and S3'. The DNAs were obtained from Integrated DNA Technologies Inc. (San Diego, CA) (for S1 and S1') and Sigma Genosys (Oakville, Ontario) (for S2, S2', S3 and S3'). S1 and S1', S2 and S2' are complementary, respectively, except for the unpaired TTT sequence at the 3' end of S1' and S2'. S3 and S3' are fully complementary. The corresponding dsDNAs are named D1, D2 and D3. The sequences and modifications of these DNA oligonucleotides are listed in Table 1. D1 and D2 are designed to have different sequences, in order to avoid any possible hybridization between S1 and S2' or between S2 and S1' in mixed solutions after D1 and D2 are dehybridized. D1 and

Table 1. **DNA oligonucleotides and corresponding modifications**

	ssDNA sequence/modification		
S1	Cy5-5'-CAT GAC CTG GAT GCA-3'		
S1'	5'-TGC ATC CAG GTC ATG TTT-3'-O-$(CH_2)_6$-S-S-$(CH_2)_6$-OH		
S2	TAMRA-5'-ATG GAT GAT GTG GTA-3'		
S2'	5'-TAC CAC ATC ATC CAT TTT-3'-O-$(CH_2)_6$-S-S-$(CH_2)_6$-OH		
S3	HO-$(CH_2)_6$-S-S-$(CH_2)_6$-O-5'-AGAGA ACC TGG GGG AGT ATT GCG GAG GAA GGT-3'-TAMRA		
S3'	5'-ACC TTC CTC CGC AAT ACT CCC CCA GGT TCTCT-3'		
	dsDNA composition	**T_m / °C**	**Length / nm**
D1	S1 + S1'	60.1	5.0
D2	S2 + S2'	53.1	5.0
D3	S3 + S3'	80.7	10.6

D2 sequences are adapted from related research of Cao et al.[80]. The D3 sequence is adapted from the adenosine aptamer sequence[81, 82]. The slight T_m difference (~ 7 ^{o}C) between D1 and D2 should not influence the laser experiments as detailed below.

$HAuCl_4$ was purchased from Alfa Aesar (99.999%, Ward Hill, MA). Other chemicals were of analytical reagent grade and used without further purifications. All solutions were prepared with deionized water (≥18.3 MΩcm) produced from a Barnstead EasyPure UV/UF compact water system (Dubuque, IA).

2.2 Synthesis and characterization of Au nanostructures

To synthesize AuNPs, 240 mg of $HAuCl_4$ was dissolved in 500 mL of water and brought to boil in a round-bottom flask on a heater with mantle. The mantle made sure that the entire solution was heated homogeneously. The solution was vigorously stirred using a magnetic bar. 50 mL of 1% (by mass) sodium citrate solution was preheated to minimize temperature gradient. When the $HAuCl_4$ solution was boiled and reflux was on, the sodium citrate solution was added abruptly. The solution color gradually changed from pale yellow to deep red, as $Au_{(s)}$ seeds grew into AuNPs. The solution was kept at boiling for one hour before allowed to cool down to room temperature.

Au nanoshells were purchased from Nanospectra Biosciences Inc. (Houston, TX). The silica core diameter was around 218 nm, while the gold shell was about 15-20 nm thick according to the information provided by the manufacturer, and confirmed by our TEM measurements.

TEM measurement was carried out on a Hitachi 8000 transmission electron microscope to determine the size and monodispersity of nanostructure solutions. A typical sample was prepared following the literature procedure[83], by dropping 5 μL of diluted nanostructure solution onto a porous carbon-coated copper TEM grid. In particular, the AuNP solution was diluted 10 times before they were deposited onto the TEM grid, in order to avoid aggregation due to high concentration. The grid was left for 10 minutes, followed by touching the edge of the grid with filter paper to wick away excess solution. The grid was allowed to dry overnight before being analyzed by TEM. TEM was operated under 200 kV voltage. AuNP was measured at 4×10^4 magnification, while AuNS was measured at 2×10^4 magnification.

2.3 Preparation and purification of dsDNA-modified Au nanostructures

This section describes the immobilization of DNA on Au nanostructure surface. In order to reduce the disulfide bonds and generate thiol-terminated ssDNA, 20 μL of 100 μM DNA oligonucleotide was treated with 20 μL of 10 mM tris(2-carboxyethyl) phosphine hydrochloride (TCEP, Aldrich-Sigma) in phosphate buffered saline (PBS: 100 mM NaCl, 10 mM phosphate buffer, pH=7.4) at room temperature for 4 hours. The function of TCEP is to cleave the disulfide bond, so that the thiol group is activated and ready to bind to the Au nanostructure[84], described as following:

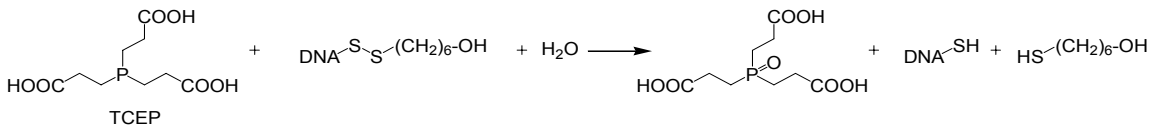

This solution was then desalted in an illustra MicroSpin G-25 Column (GE Healthcare, Buckinghamshire, UK). This G-25 column is used to separate DNA from the DNA labeling reaction[85]. It contains Sephadex™ G-25 DNA grade F resin, which allows DNA purification by the process of gel filtration. Molecules larger than the largest pores in the Sephadex are excluded from the gel and elute first (purified DNA oligonucleotide). Intermediate size molecules penetrate the matrix to varying extents, depending on their size and the resin used. Penetration of the matrix retards progress through the column; very small molecules elute last (excess TCEP and HS-$(CH_2)_6$-OH). To purify DNA, first the resin in the column was suspended by vortexing, followed by centrifuging the column at 735 g for 1 minute. The DNA solution was carefully loaded to the top-center of the resin, and then centrifugation was carried out again at 735 g for 2 minutes to elute.

This aliquot of purified thiol-terminated ssDNA strands were then hybridized with 20 µL of 100 µM of their complementary strands (S1-S1' forms D1, S2-S2' forms D2, S3-S3' forms D3, respectively) by heating at 85 °C for 5 minutes and being allowed to slowly cool to room temperature for 1 hour.

Coupling of DNA oligonucleotides and Au nanostructures was performed following the procedure reported by Rosi et al[86]. 2 nmol of hybridized dsDNAs were incubated with 0.8 mL of argon-purged AuNP or AuNS solution. After 20 minutes, 10 µL of sodium dodecyl sulphate (SDS, 10% solution in water), 100 µL of phosphate buffer (0.1 M; pH = 7.4) and 50 µL of 2.0 M sodium chloride were added for salt aging. SDS acts as a surfactant to prevent AuNPs aggregating at

high salt concentration. This solution was sonicated for 10 seconds and then mounted on a vortexer and shaken gently for 30 minutes. Afterwards addition of 50 μL of 2.0 M sodium chloride and 10 seconds of sonication were repeated twice in a 30 minute interval. This final solution was gently shaken overnight to complete the oligonucleotide functionalization. The product was then centrifuged at 13,000 rpm for 20 minutes, so that nanostructures precipitated from solution. After centrifugation, the supernatant was discarded and 0.8 mL of fresh PBS solvent was added to the nanostructure precipitate. The nanostructures were then re-suspended by vortexing and 10 seconds of sonication[87]. This centrifugation was repeated twice to separate DNA-Au nanostructures from the remaining free DNAs in the immobilization solution. After centrifugation, only immobilized DNAs (FL was quenched) were expected to be present, while free DNAs (high FL) were supposed to be discarded. FL was measured to assure minimum FL signal presented in the sample after centrifugation, i.e. most free DNAs were separated from solution.

UV absorbance spectra were recorded on a QE65000 Scientific-grade Spectrometer (Ocean Optics, Inc.) with a DH-2000-BAL Deuterium Tungsten Halogen Light Source, which produces stable output from 215-2000 nm. FL spectra were recorded on a LPS-220B fluorescence spectrometer (Photon Technology International). Grating was set to 2 nm, step size was 0.25 nm and integration time was 0.25 second. Excitation wavelength was 633 nm for Cy5 and 550 nm for TAMRA.

2.4 Laser setup for sample irradiation

Laser is an acronym for Light Amplification by Stimulated Emission of Radiation. A laser consists of three principle parts: pump source, gain medium and optical cavity. The pump source provides energy to the laser system. The source could be electrical discharges, flash lamps, etc. The gain medium is excited by the pump source to produce a population inversion, leading to amplification. The optical cavity can be viewed as two parallel mirrors placed around the gain medium, one highly reflective, one partially transparent. The latter allows some of the photons to leave the cavity, producing the output laser beam.

If light (photons) from the pump source pass through the gain medium, there is a possibility of the light being absorbed by the atoms of the gain medium, which are originally in the ground state. This will cause electrons to be excited to the higher energy state. There are two routes by which the atoms come back to the ground state, namely spontaneous emission and stimulated emission.

In spontaneous emission, the atoms spontaneously decay from the excited state to the ground state, and the energy difference is emitted as a photon. Spontaneous emission is incoherent.

If an atom in the excited state is perturbed by a photon (the photon frequency must match the energy gap between the excited state and the ground state), the atom comes back to the ground state, emitting a second photon of the same frequency. On the other hand, the first photon is not absorbed. This produces two coherent photons, thus called stimulated emission. These photons

travel back and forth between the two mirrors, thus pass through the gain medium multiple times, thus produce more and more coherent photons. This is how laser is amplified.

When a photon travels through the gain medium, it could perturb an atom in the excited state to induce stimulated emission, but it could also be absorbed by an atom in the ground state, in which case the photon is lost. Therefore the key to produce laser amplification is to have more atoms in the higher (excited) state than in the lower (ground) state (this phenomenon is called population inversion). In a group of atoms only has two energy levels, because of the spontaneous and stimulated emission from excited state to ground state, the number of atoms in the ground state is always larger than that in the excited state. In other words, population inversion cannot be achieved.

In order to populate the excited state, a three-level laser is used (Fig. 2.1). Level 1 is the ground level, while levels 2 and 3 are the excited levels. After the atoms are pumped from level 1 to level 3, most of the atoms are transferred by fast radiationless transitions into the intermediate level 2. In this process the energy is transferred to the lattice. Finally, the electrons return to level 1 by the emitting photons, which corresponding to laser transition. In this model, because the radiationless transition is faster than the laser transition, more and more atoms (coming from level 3) stay in level 2, resulting in a population inversion between level 1 and level 2. A four-level laser system can also be built based on

the same mechanism.

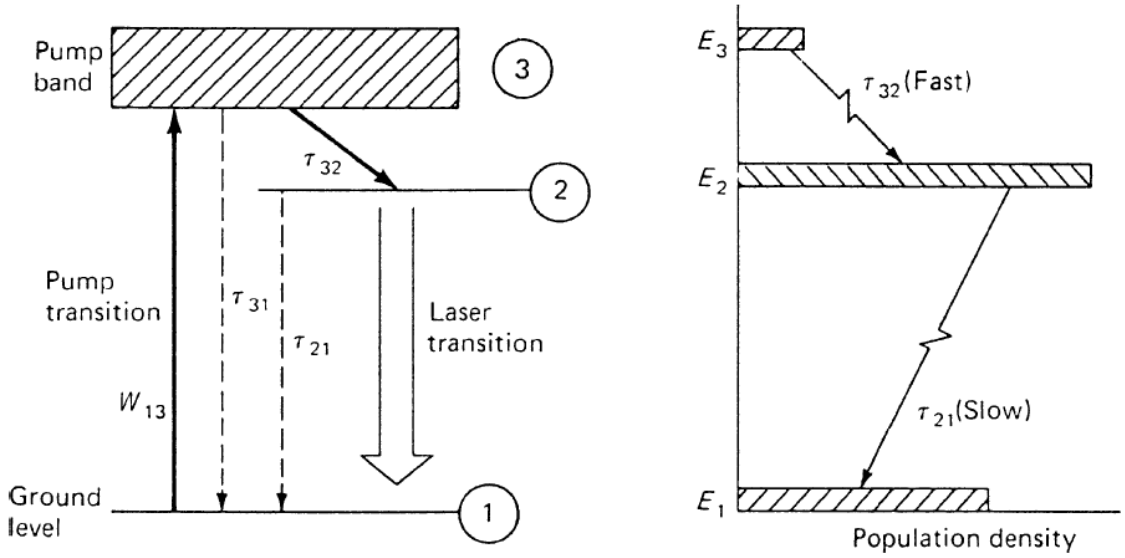

Figure 2.1 Simplified energy level diagram of a three-level laser. Adapted from reference 88.

In the instrumental setup, a nanosecond Nd:YAG laser (Continuum Powerlite Precision II 8000, Santa Clara, CA) was used to irradiate DNA-Au nanostructure conjugates. It emits infrared light at 1064 nm. In order to tune the power of the laser pulse, the laser pulse that comes out of the optical cavity (through the Output Coupler, component 6 in Fig. 2.2) passes through the amplifier (a flash lamp) (component 8 in Fig. 2.2). If the laser pulse passes through the lamp when there is a peak of the flashing pulse, it acquires more energy and becomes amplified; If it is phase-shifted, the incoming pulse does not meet the flashing pulse, then the laser power stays unchanged. An example of how laser is amplified can be found in reference 88, 89. 1064 nm is the fundamental wavelength of the laser, but the pulse can be frequency doubled in a second-harmonic generator (SHG) to generate a green beam at 532 nm. A

second-harmonic signal is generated when two near-infrared photons interact with a highly polarized and noncentrosymmetric material (potassium dideuterium phosphate is used in my setup). This interaction generates a single, visible photon having twice the energy and half the wavelength[88, 90, 91].

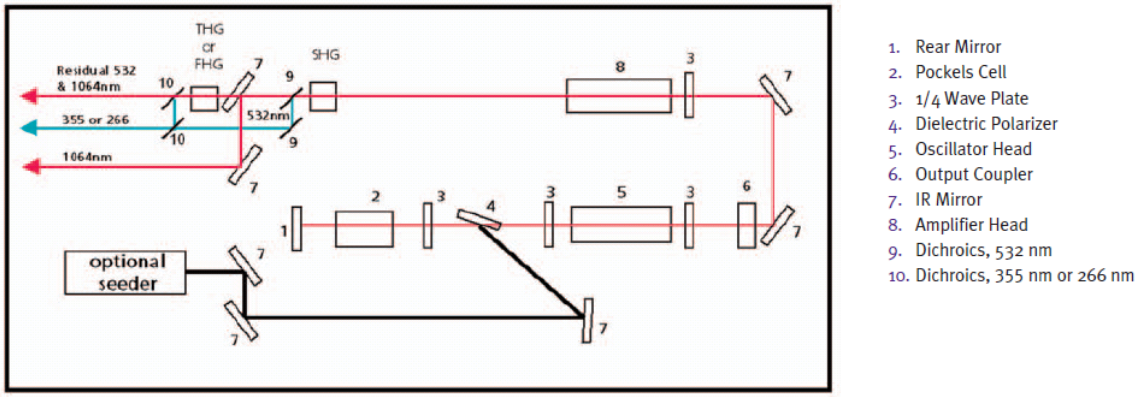

Figure 2.2 Continuum Powerlite Precision II 8000 laser optical layout. Adapted from reference 92.

Typically, 200 µL of 1.02 nM AuNP-D1 solution and 200 µL 0.25 pM of AuNS-D2 solution were mixed and centrifuged. The precipitate was redispersed in 200 µL of PBS. 5 µL of 10% (by mass) SDS was added to 50 µL of this mixed solution in a FL cuvette with interior footprint of 3×3 mm^2. To minimize inconsistency, the cuvette was put in a holder in a fixed position in the path of the laser beam. The generated laser beam had a diameter of 8.0 mm and position of the cuvette was adjusted so that the solution was exposed to the center of the laser beam (Fig. 2.3). Separate samples (containing only 1.02 nM of AuNP-D1 or 0.25 pM of AuNS-D2 conjugates) were also prepared by adding 5 µL of 10% SDS to 50 µL of the respective solutions.

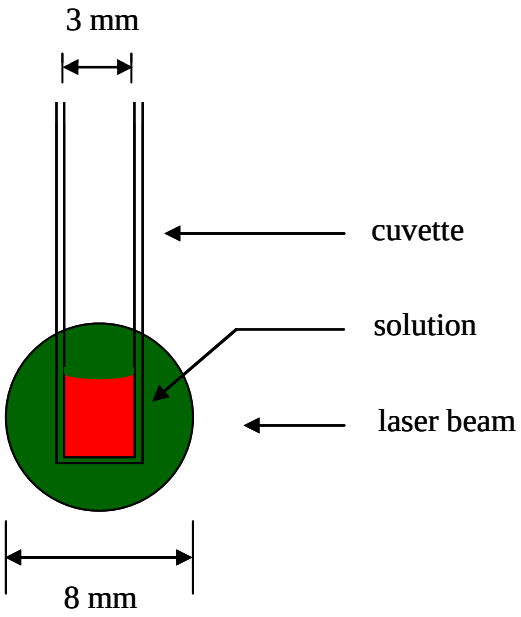

Figure 2.3 Position of cuvette in the laser beam.

3: RESULTS AND DISCUSSION

3.1 Design and preparation of DNA-Au nanoconjugates for the laser-induced selective dehybridization experiments

We started by preparing two dsDNA sequences of 15 base pairs. As listed in Table 2.1, in each dsDNA, one strand (S1 or S2) was modified with a TTT spacer and thiol group, by which the dsDNA could covalently bind to Au nanostructure via an Au-S linkage. Their complementary strands (S1' and S2') were modified with fluorophores (Cy5 or TAMRA) for FL detection. These two dsDNAs were immobilized on two kinds of Au nanostructures. One type is gold nanoparticle (AuNP) with peak absorbance at 520 nm. The other is Au/SiO_2 nanoshell (AuNS) with peak absorbance at 1100 nm. As shown in Fig. 3.1, upon immobilization on Au nanostructures, the fluorophores were close to the nanoparticles, therefore the FL was quenched. We expected that the laser-induced selective dehybridization should occur at certain wavelengths. For example, the 532-nm laser would "excite" the AuNP, therefore dehybridize the attached D1 dsDNAs, while the 1064-nm laser would dehybridize D2 dsDNAs on AuNS. The detachment of the fluorophore-tethered DNA strands from the gold nanostructure surface should give rise to a FL signal. Since Cy5 and TAMRA have different emission wavelengths, we should be able to determine which fluorophore has left the nanostructure, thus confirming the selective dehybridization process.

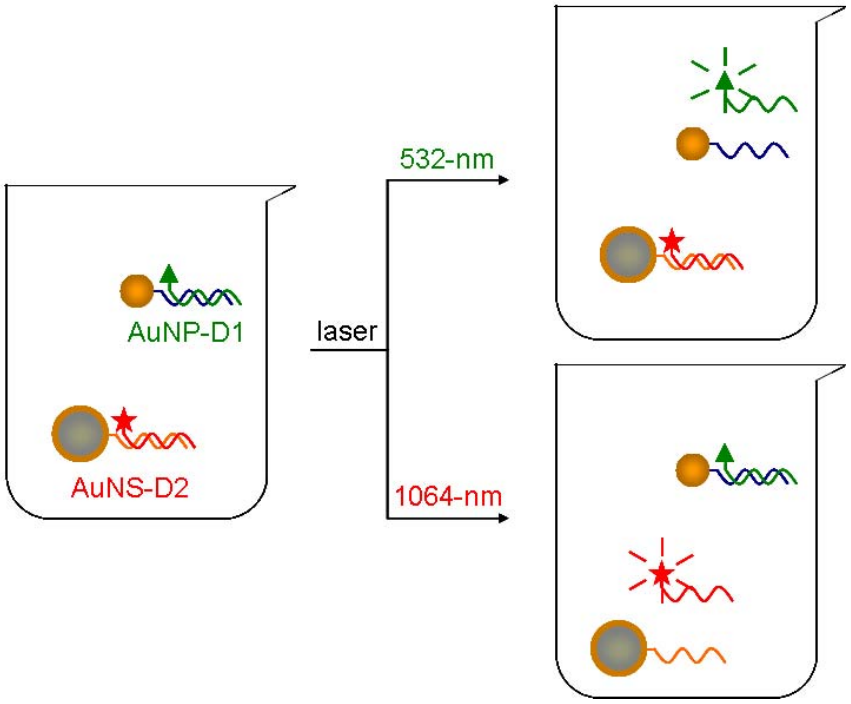

Figure 3.1 A mixture of two DNA-Au nanoconjugates being selectively dehybridized by laser irradiation at different wavelengths. When irradiated with a 532-nm laser, only D1 is dehybridized, for which the Cy5 FL intensity increases. When irradiated with a 1064-nm laser, only D2 is dehybridized, leading to an increased TAMRA FL signal.

3.2 Laser induced dehybridization of DNA-Au nanostructures

3.2.1 Characterization of Au nanostructures and DNA-Au nanoconjugates

The AuNP was synthesized by following the procedure described in Chapter 2. The concentration of AuNP in the original solution was determined by measuring the peak absorbance at 520 nm (Fig. 3.2), according to equation 2

$$A = \varepsilon bc \qquad (2)$$

where ε is the extinction coefficient of AuNP, b is the path length (3 mm) and c is concentration. For AuNP of a diameter of 24 nm, ε is 2.9×10^9 M^{-1} cm^{-1} according

to the literature[57]. The maximum absorbance of typical AuNP solutions as prepared was measured to be in the range of A = 1.4 at 520 nm, giving a concentration of 1.6 nM. The absorbance value is high, but still in the linear range as confirmed by a series of dilution experiments. The high ε value of AuNP is the reason for which low concentration can produce high optical absorbance. Both the absorbance value and concentration are consistent with the results of Liu et al.[57] At the wavelength of the laser used for the dehybridization experiments, the absorbance is about 95% of the peak value (A_{532nm} / A_{520nm} = 95%), which ensures that AuNP is efficiently "excited" by the 532-nm laser.

The concentration of the original AuNS solution was calculated from the NIR absorbance (A) at 1095 nm. The ε value is 4.0×10^{11} M^{-1} cm^{-1} according to the product information provided by the supplier. A typical AuNS sample (A_{1095nm} = 0.097 as shown in Fig. 3.2) concentration was calculated to be 0.83 pM. According to the supplier this is the maximum concentration for AuNS of this size without causing aggregation or precipitation. The high absorbance at 1064 nm (the laser wavelength that will be used for the dehybridization experiments) (0.096, 99% of A_{1095nm}) ensures that AuNS can be efficiently "heated" by the laser. The measured maximum absorption and the peak position above are also in line with the values reported in the literatures for AuNSs of similar sizes and compositions[17, 25, 65]. The moderate absorbance in the broad 700 - 950 nm region can be attributed to the quadrupolar oscillations in the nanoshells of large sizes[17, 93, 94]. AuNS has relative low absorbance at 532 nm, suggesting that the 532-nm

laser should not heat AuNS to as high temperature as 1064-nm laser (discussed in Section 3.2.3).

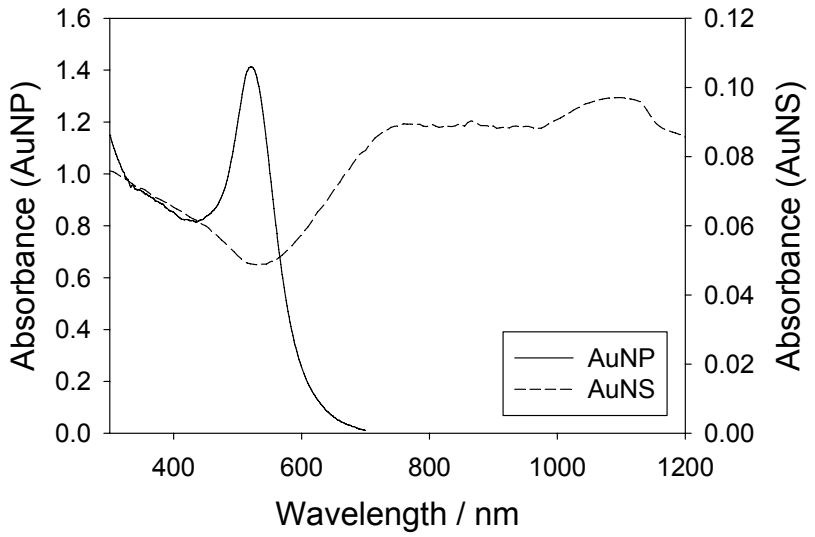

Figure 3.2 UV/Vis/NIR absorbance spectra of typical samples of AuNP (solid line) and AuNS (dashed line).

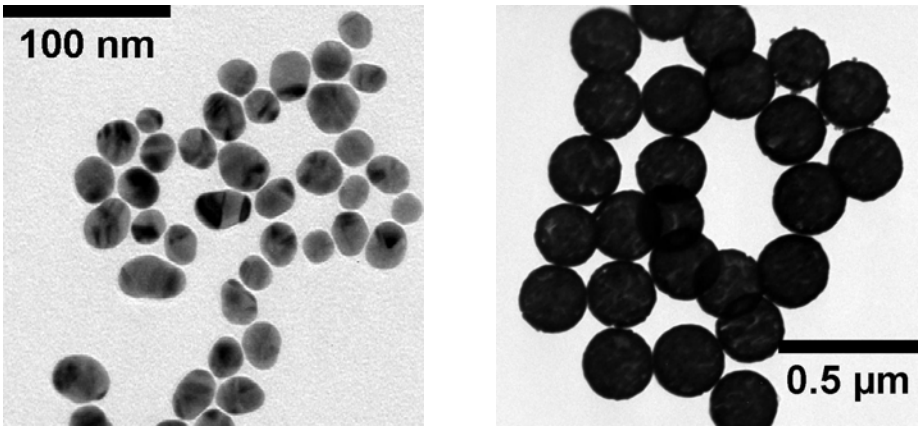

Figure 3.3 TEM images of AuNPs (left) and AuNSs (right).

TEM images of AuNPs and AuNSs were obtained to confirm their size and uniformity (Fig. 3.3). As shown in the TEM image, the AuNSs are uniform and have a small size distribution. The AuNPs vary more in terms of relative size

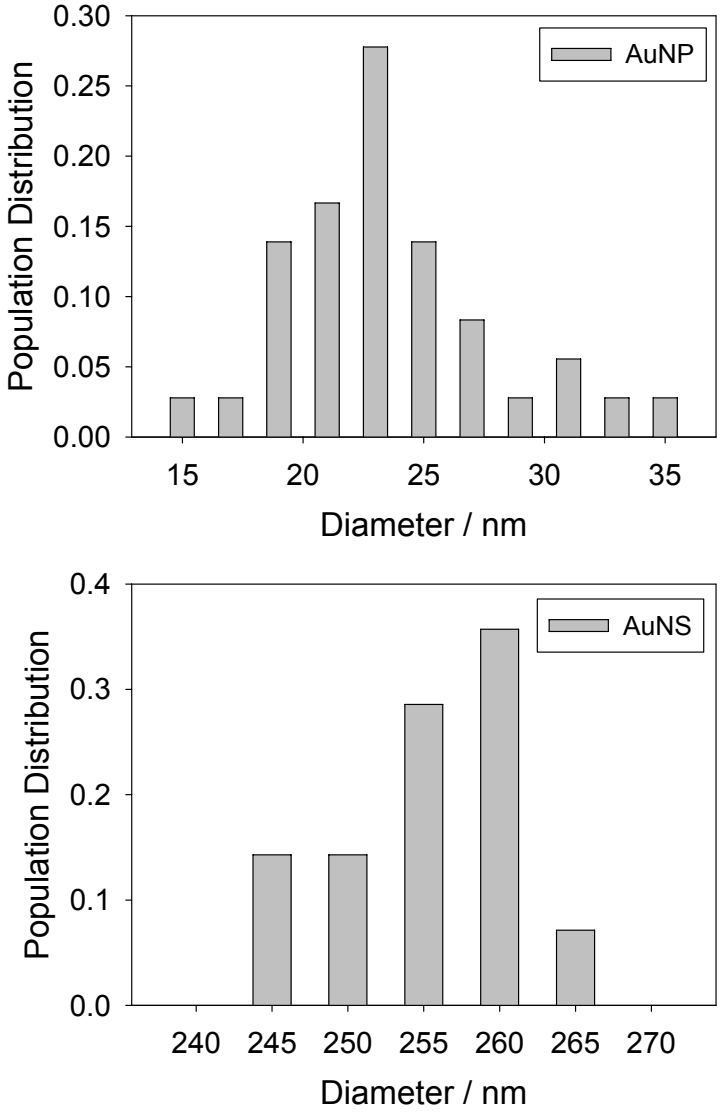

Figure 3.4 Diameter distributions of typical samples of AuNP (up) and AuNS (down) as obtained by using ImageJ software to analyze the TEM images. AuNSs are very uniform (253 ± 5 nm) while AuNPs had a slightly broader size distribution (24 ± 4 nm).

distribution than AuNSs, but not to the extent that absorption peak would be broadened (Fig. 3.2). The diameter is 24 ± 4 nm for AuNP and 253 ± 5 nm for AuNS, as measured by the TEM and processed by ImageJ software (Fig. 3.4). The average of maximum and minimum diameters is used as diameter of the non-spherical AuNPs.

Due to partial loss of particles in the immobilization procedure, the concentrations of both nanostructures decreased. The AuNS-D2 sample was concentrated four times by centrifugation and redispersed to maintain a high AuNS-D2 concentration, in the hope of obtaining high FL signal from D2 when dehybridized. Absorbance spectra were measured to determine the concentrations again (Fig. 3.5). The AuNP-D1 peak absorbance was typically measured as A = 0.96 at 527 nm, giving an AuNP-D1 concentration of 1.1 nM. This means 69% of particles remained in the solution after immobilization, compared to that before the dsDNA immobilization. The AuNS-D2 peak absorbance was typically measured as A = 0.21 at 1120 nm, giving an AuNS-D2 concentration of 1.8 pM. This means 55% of AuNS remained in the solution. These percentages are reasonable as a fair amount of nanostructures were lost during the three rounds of separation of supernatant and precipitate (Section 2.3). Compared with the unmodified nanostructures, AuNP peak shifted from 520 nm to 527 nm, AuNS from 1095 nm to 1120 nm. In general, the peak shift is due to the changes in the immediate environment of nanostructures, the immobilization of DNA oligonucleotides in the present system. The same phenomenon (peak shift) has been reported in literature[95]. TEM images were

taken again (Fig. 3.6); no discernible changes are evident either in the monodispersity or the particle size (compared with Fig. 3.3). As shown in the TEM images, the gold nanostructures tend to stack on each other. The stacking is possibly caused by the increase in concentration during the process of gradual drying after the Au nanostructure solution being dropped onto the TEM grid.

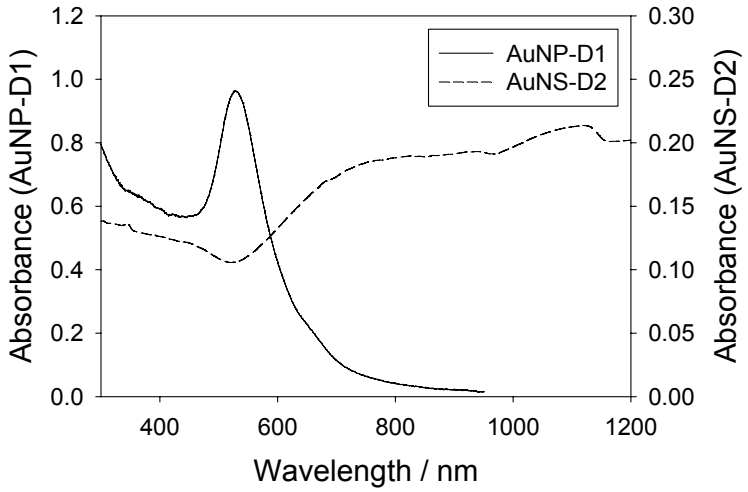

Figure 3.5 Optical absorbances of typical samples of AuNP-D1 (solid line) and AuNS-D2 (dashed line).

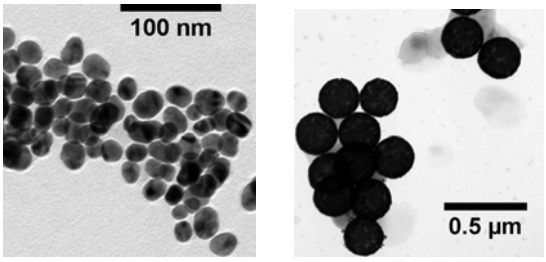

Figure 3.6 TEM images of DNA-Au nanoconjugates: AuNP-D1 (left) and AuNS-D2 (right).

The concentrations of the D1 and D2 DNAs in the AuNP-D1 and AuNS-D2 solutions were also measured. In the process of immobilization of DNA on nanostructure surface, the same DNA/nanostructure ratio was used to mix DNAs

and nanostructures in each batch (400/1 for D1/AuNP, 1.0×10^6/1 for D2/AuNS). However, the final surface density of DNAs that were actually immobilized on each nanostructure varied. The D1 concentration was measured at 3 ± 1 nM, while the D2 concentration at 1.24 ± 0.06 nM (based on three trials). The "final" DNA/nanostructure ratio is 3/1 (± 34%) for AuNP-D1 and 7×10^2/1 (± 5%) for AuNS-D2.

3.2.2 532-nm laser induced AuNP-D1 dehybridization

As mentioned in Section 2.1, the S1 strand is labeled with a Cy5 fluorophore, which has the maximum absorption at 648 nm and maximum emission at 668 nm. Because the AuNP is highly scattering, a part of the excitation light was scattered into the emission window and shown in the fluorescence spectrum[17]. In my experiment when the excitation wavelength was set to 648 nm, the scattering (peak at 648 nm) had a strong contribution at 668 nm, as the two wavelengths are only 20 nm away. Since the scattering peak is always located at the excitation wavelength, we shifted the excitation wavelength from 648 nm to 633 nm. By doing so, the scattering was minimized as its peak was shifted away from the FL peak.

The changes in the FL spectra and relative FL intensity changes of AuNP-D1 upon laser irradiation are presented in Fig. 3.7. The FL intensity of the AuNP-D1 sample is weak before laser irradiation. Upon irradiation with the 532-nm laser (357 mW, 5 min), the FL intensity became much stronger (the red curve), notably the maximum emission was still observed at 668 nm (characteristic of the Cy5 fluorophore). We believe that the increase of FL intensity is due to the fact

that S1 DNA strands are diffusing away from the quencher (AuNP), as the laser irradiation heats up the AuNP and subsequently dehybridizes the attached dsDNAs. In contrast, when the sample was irradiated with 1064-nm laser (502 mW, 5 min), no significant change in the FL spectrum was observed. In this particular case, a small decrease in the FL intensity was observed. Since DNA/gold nanoparticle ratio varies for different batches of solutions (from 9×10^4 to 2.1×10^5 counts/s), the relative FL intensity increase $\Delta I/I_0$ was plotted in Fig. 3.7b, where I_0 represent the FL intensity before laser irradiation. By doing this, the FL signals from different trials can be directly compared. Fig. 3.7b shows that the irradiation with the 532-nm laser at 300 mW led to a remarkable increase of FL intensity ((148±76)% higher than the original signal). This increase is clear evidence that the AuNP-D1 dehybridizes upon irradiation by 532-nm laser, which does not happen if irradiated with a 1064-nm laser.

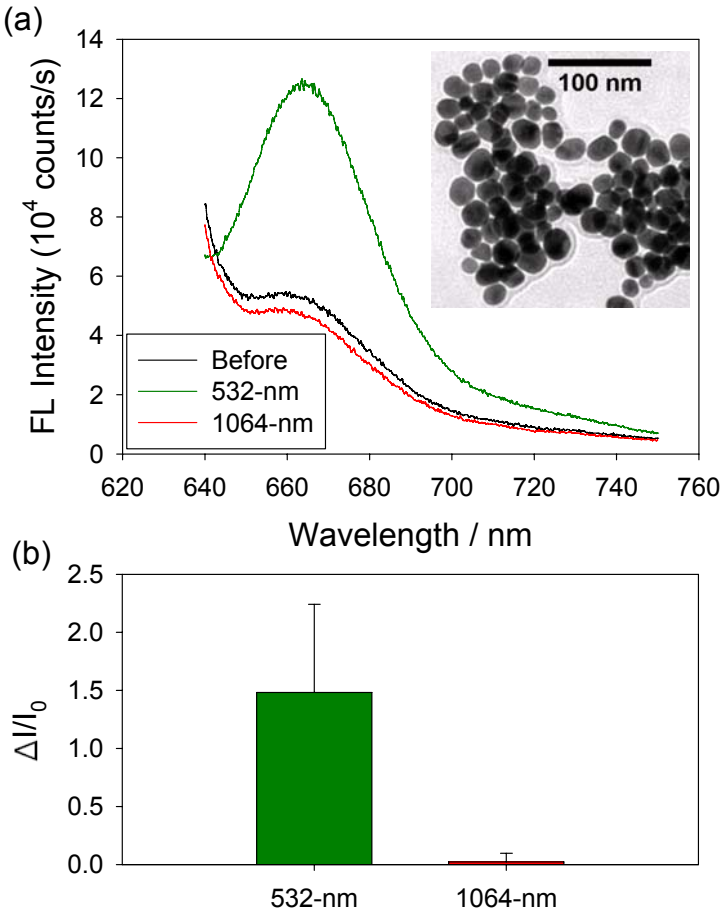

Figure 3.7 AuNP-D1 irradiated with 532-nm laser. Excitation wavelength: 633 nm; Irradiation time: 5 min; laser power: 300 mW (532-nm laser) and 500 mW (1064-nm laser). (a) FL intensity vs. wavelength in a typical sample as AuNP-D1 is irradiated by 532-nm laser and 1064-nm laser (as comparison). Insert: TEM image of AuNP-D1 after laser irradiation. (b) Averaged relative FL intensity increase after laser irradiation. The error bars represent the standard deviations from six independent samples.

In principle, the increase of FL intensity can be a result of the following: firstly, due to the dehybridization of dsDNA the Cy5-labeled S1 strands are released into the solution, as we expected and mentioned above (Fig. 3.1); secondly, the Au-S bond between the AuNP and the S1 strands are cleaved, so that the dsDNAs leave the AuNP[38]; finally, AuNP may be melted under high

power laser irradiation, which “naturally” releases all the DNAs attached to it, whether dehybridized or not[22]. The second possibility will be discussed and experimentally tested in greater detail in Section 3.2.4. To rule out the last possibility, TEM images were recorded (inset Fig. 3.7a) after the laser irradiation. Compared with the original AuNP-D1 TEM image in Fig. 3.6, no aggregation was observed (no large particles forming), indicating that the AuNPs remained intact upon laser irradiation.

Recently, Bakhtiari et al. have shown that localized heat generated by the photothermal effect of Au nanoparticles can selectively cleave the chemical bonds and trigger the retro-Diels-Alder reaction[96]. The manipulation of DNA dehybridization is one step further in this field, as it needs a definite control of the photothermal effect. Although the release of DNA strands via cleavage of the Au-S bond or melting of the Au nanostructure have been reported by other groups[22, 38], it should be emphasized that neither the Au-S bond nor the Au nanostructures are damaged in my study. In contrast, in the work by Wijaya et al.[22] the nanorods are melted and destroyed by high laser power in order to release the attached DNA strands. In my study, DNA strands are released while the AuNPs are intact and the single-stranded DNA tethered Au nanoparticles may be used again for the same type of experiments.

Fig. 3.8 shows the dependence of the dehybridization percentage on the laser power used to irradiate AuNP-D1. When the power was set low (below 100 mW), a minimal FL increase was observed; from 100 mW to 300 mW, the FL intensity increased monotonically as the laser power increased; above 300 mW,

the FL signal reached its maximum, indicating that the dehybridization percentage does not increase anymore. This trend shows that 1) when laser power is lower than 100 mW, the local temperature is lower than T_m, hence no dehybridization occurs. 2) From 100 mW to 300 mW, more and more AuNPs are heated up to the T_m. AuNPs with different size and shape might need different laser power to reach the T_m, thus a power range is present. 3) When laser power is higher than 300 mW, most of the D1 DNAs are dehybridized. Fig. 3.8 demonstrates that we are capable of controlling the percentage of DNAs that are released from the nanostructure by adjusting the irradiation laser power. It is noted that when the laser power was high (above 300 mW), the FL signal started to fluctuate, and considerable variations among different trials were observed. Under extremely high power (>600 mW), it was discovered that the solution became colorless and the AuNP-D1 sank to the bottom of the cuvette (cannot be recovered by sonication), therefore the FL signal decreased sharply. This could be due to the AuNP-D1 aggregation under high laser power (data not shown).

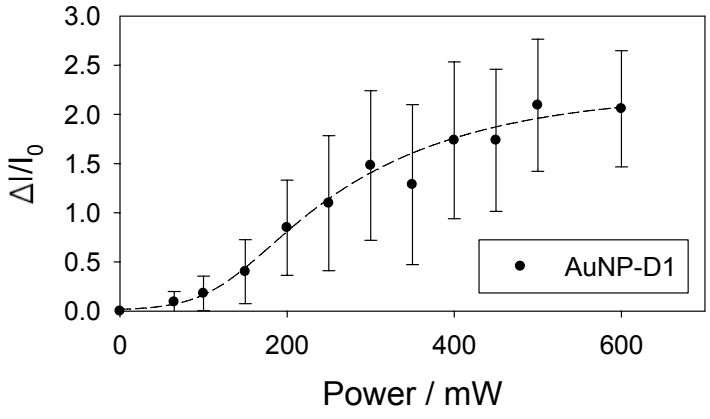

Figure 3.8 The power dependence of the laser induced dehybridization of AuNP-D1. Irradiation time: 5 min. The dashed line is a guide to eyes only. The error bars represent the standard deviations from six independent samples.

For a better control of dehybridization conditions, the effect of irradiation time was also studied. It has been proposed that gold nanostructures can be heated up within picosecond timeframe[72]. However, in order to build up the temperature of the local environment to above T_m (60.1 °C in this case), multiple pulses might be needed, hence longer irradiation time. Furthermore, DNA dehybridization is a reversible process, which means that the released S1' ssDNA may rehybridize with the surface-attached S1 strands[69, 74]. In this regard, the laser irradiation time should be long enough so that the released S1' strands would be able to diffuse away from the AuNP surface (into the bulk solution). As shown in Fig. 3.9, initially the dehybridization percentage increases with increasing irradiation time, and remains constant after 300 seconds. In this case, the FL intensity no longer increases when irradiated for a longer period of time. The time dependence indicates that the dehybridization might be dictated by the

DNA diffusion into the bulk solution, instead of the heat transfer from AuNP to DNA. The relative FL intensity increase $\Delta I/I_0$ (defined as I') as function of irradiation time (t) fits in the equation:

$$I' = I'_0 + a(1 - e^{-kt}) \quad (3)$$

The fitting parameters are $I'_0 = 0.36$, $a = 4.9$, $k = 0.0053\ s^{-1}$ ($R^2 = 0.99$). This shows that the reaction:

$$\text{AuNP-D1} \leftrightarrow \text{AuNP-S1} + \text{S1'}$$

can be considered as a first-order reaction on the AuNP surface. This is in accordance with the result of Wetmur et al.[97], where the kinetics of DNA dehybridization was discussed in detail. Temperature of the solution was measured before and after laser irradiation and found no change, which proves that only the local environment, not the entire solution, is heated by laser irradiation.

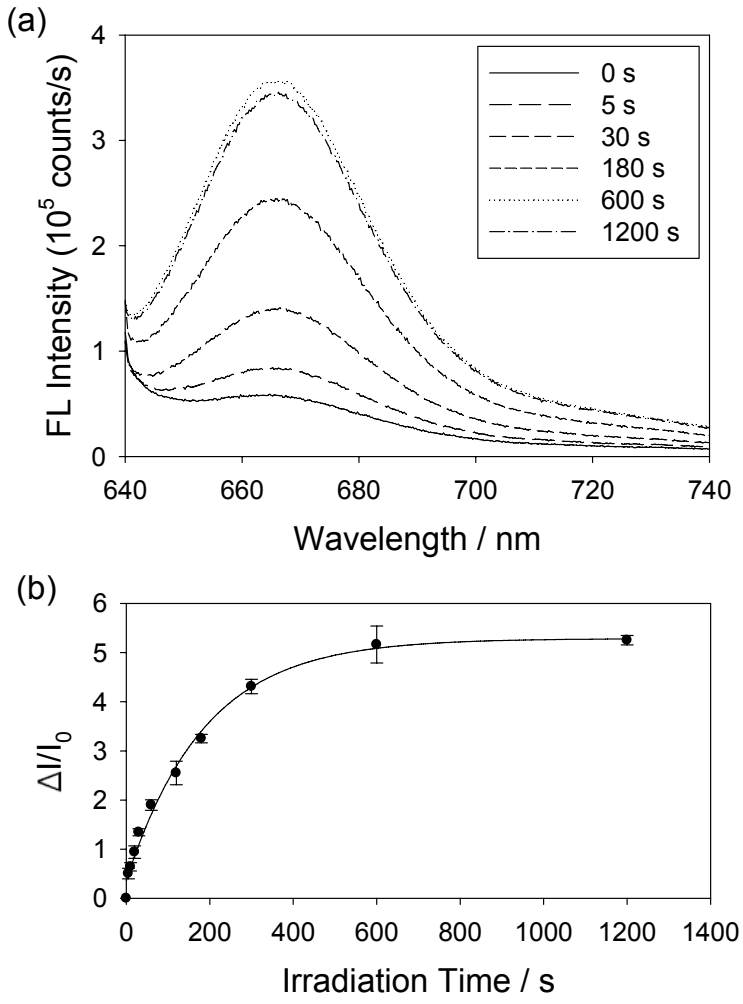

Figure 3.9 Irradiation time-dependence of AuNP-D1 dehybridization by 532-nm laser at 300 mW. (a) FL intensity vs. wavelength in a typical sample. (b) Averaged relative FL intensity increase vs. irradiation time. The error bars represent standard deviation (based on 3 trials).

3.2.3 1064-nm laser induced AuNS-D2 dehybridization

The 5' end of the S2 DNA is modified with a TAMRA fluorophore that has a maximum absorption is at 555 nm and maximum emission at 580 nm. To avoid strong contribution of scattering, the excitation wavelength is shifted from 555 nm to 550 nm. Fig. 3.10 shows the results of AuNS-D2 dehybridization upon

irradiation with 1064 nm laser. Relatively weak initial FL intensity was measured at 574 nm (Fig. 3.10a, black curve). When the AuNS-D2 was irradiated with a 1064-nm laser at 250 mW for 5 min, the FL intensity increased significantly (Fig. 3.10a, red curve). In contrast, there was only a minimal increase of the FL signal when the solution was irradiated with a 532-nm laser (300 mW, 5 min). Since AuNS has moderate absorbance at 532 nm (Fig. 3.2), it might have been photothermally heated up (but to a lesser extent). Fig. 3.10b shows a direct comparison of the relative FL intensity increase: 1064-nm laser irradiation increases the FL signal by 56±5%, which is much higher than the increase caused by the 532-nm laser (14±7%). The 14±7% increase caused by the 532-nm laser is possibly due to the reasonable AuNS absorbance at 532 nm (Fig. 3.2). According to Fig. 3.2, AuNS can be partially heated by 532-nm laser, reducing the selectivity of laser irradiation. But as experimental data shows, the photothermal effects of 1064-nm laser on AuNS-D2 and AuNP-D1 are distinguishable in general.

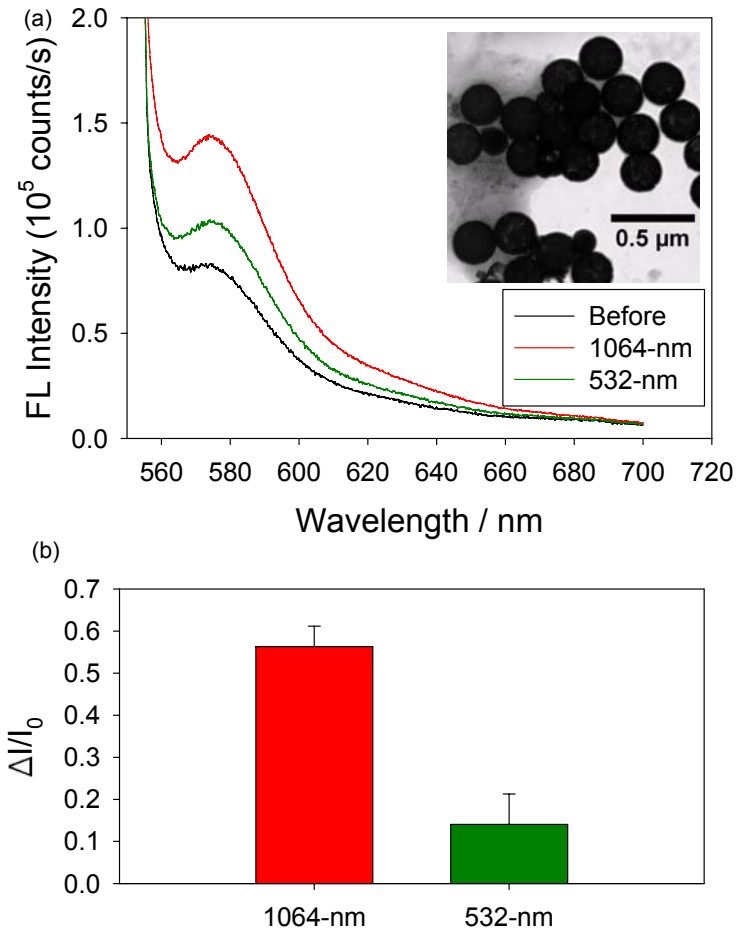

Figure 3.10 AuNS-D2 irradiated with 1064-nm laser. Excitation wavelength: 550 nm; Irradiation time: 5 minutes; laser power: 250 mW (1064-nm laser) and 300 mW (532-nm laser). (a) FL intensity vs. wavelength in a typical sample as AuNS-D2 is irradiated by 1064-nm laser and 532-nm laser (as comparison). Insert: TEM image of AuNS-D2 after laser irradiation. (b) Averaged relative FL intensity increase after laser irradiation. The error bars represent standard deviation (based on 6 trials).

The power dependence of the laser-induced dehybridization of AuNS-D2 is presented in Fig. 3.11. The amount of dehybridized DNA increases gradually when laser power increases, and starts to saturate when power exceeds 300 mW. This trend is similar to AuNP-D1 (Fig. 3.8). They show a certain energy threshold behavior, particularly for AuNS-D2 at ~300 mW. They also demonstrate

that it is possible to control the DNA release process, where we can achieve a certain percentage of DNA dehybridized by adjusting the laser power.

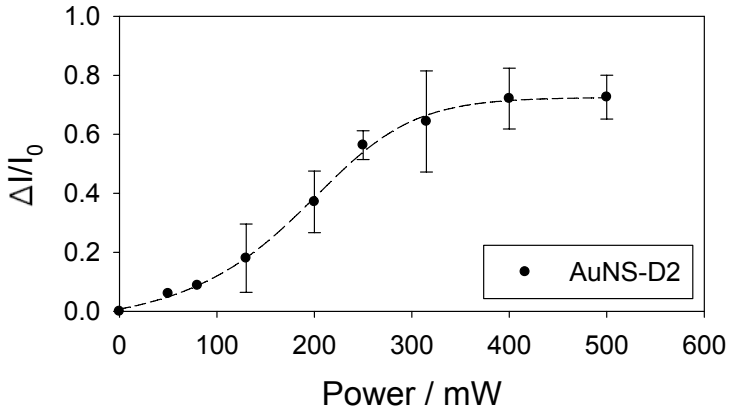

Figure 3.11 1064-nm laser power dependence for AuNS-D2. Irradiation time: 5 minutes. The dashed line is a guide to eyes only. The error bars represent standard deviation (based on 3 trials)

In principle, AuNS can be designed with higher SPR heating efficiency by fine-tuning the size and composition [71, 98]. According to Schelm et al.[98], smaller AuNS is preferred, as it absorbs more incident light and scatters less compared with larger AuNS. However, smaller AuNS may have higher absorbance at 532 nm, so the selectivity between 532-nm and 1064-nm laser irradiation experiments (described below) may not be feasible.

3.2.4 Control experiments

As discussed in Section 3.2.2, FL increase can be triggered from three possible reasons. In particular, the laser power may be high enough to cleave the Au-S bond between the AuNP and the S1' DNA strands, so that the dsDNAs are removed from the AuNP accordingly[22, 99, 100]. This type of "complete removal"

(instead of dehybridization) of dsDNA from the Au nanostructure surface also leads to an increase in the FL signal intensity. To confirm that the laser power employed in this study is not high enough to cleave the S-Au bonds, we have compared with two recent studies[72, 73]. Jain et al.[72] have determined the pulse power density that damages the thiol bond is 10^3 MW/mm^2. To calculate pulse power density in this work, P_M = 300 mW was used as the average power. Other parameters included laser pulse frequency f = 10 Hz; pulse peak width at half height w_h = 5.0 ns; laser beam radius R = 4.0 mm. The energy of each pulse is

$$E_{pulse} = P_M/f = 300/10 = 30 \text{ J}, \quad (4)$$

the pulse power is

$$P_{pulse} \approx E_{pulse}/w_h = 30/5.0\text{x}10^{-9} = 6.0\text{x}10^9 \text{ W}, \quad (5)$$

and the pulse power density is

$$I_M = P_{pulse}/\text{area} = 6.0\text{x}10^9/(3.14\text{x}4.0^2) = 1.2\text{x}10^8 \text{ W/mm}^2 = 120 \text{ MW/mm}^2. \quad (6)$$

This is much lower than the “destructive” pulse power density (10^3 MW/mm^2), confirming that the laser power we have chosen is in the “safe” range (i.e., not destructive to the S-Au bond).

At the beginning of my project, a femtosecond laser and a picosecond laser were also tested. In both lasers, at a lower laser power, no dehybridization was observed. When laser power increased to over 300 mW, we observed solution color change from dark red to colorless, and Au precipitate appears at the bottom of the cuvette. This indicates the AuNP-D1 conjugates were destroyed. Using the same equations above, pulse power densities can be

calculated as $1.2x10^8$ MW/mm^2 for femtosecond laser and $1.2x10^5$ MW/mm^2 for picosecond laser. Both values are higher than the “destructive” pulse power density (10^3 MW/mm^2), so the S-Au bond was cleaved and AuNPs precipitated.

Although the calculation as well as the TEM images and absorbance spectra can confirm that the Au nanostructures were not melted nor damaged, it is important to provide direct evidence to eliminate the possibility of dsDNA desorption.

A dual-labeled 32-base oligonucleotide S3 was prepared, with its 5’ modified with a thiol (to link DNA to AuNP), and 3’ modified with a fluorophore (TAMRA). S3 was hybridized with the fully complementary strand S3’ to form D3 and immobilized on the AuNP. The preparation of the AuNP-D3 follows the same protocol of AuNP-D1. During the laser irradiation, we expect that the S3’ strand leaves the nanoparticle, while the S3 strand stays on the nanoparticle surface. The sample solution was then centrifuged, precipitating the nanoparticles from the solution. Upon separating the precipitate (containing AuNP-S3) and supernatant (containing S3’), the precipitate was re-dispersed in PBS buffer. The FL intensities of both supernatant and re-dispersed precipitate were measured. High FL intensity in the precipitate means that the S3 strand did not leave the nanoparticle and that the Au-S covalent bond is intact. If a FL signal is observed in the supernatant, we can conclude that the Au-S bond has been cleaved, releasing the S3 strands to the solution (Fig. 3.12).

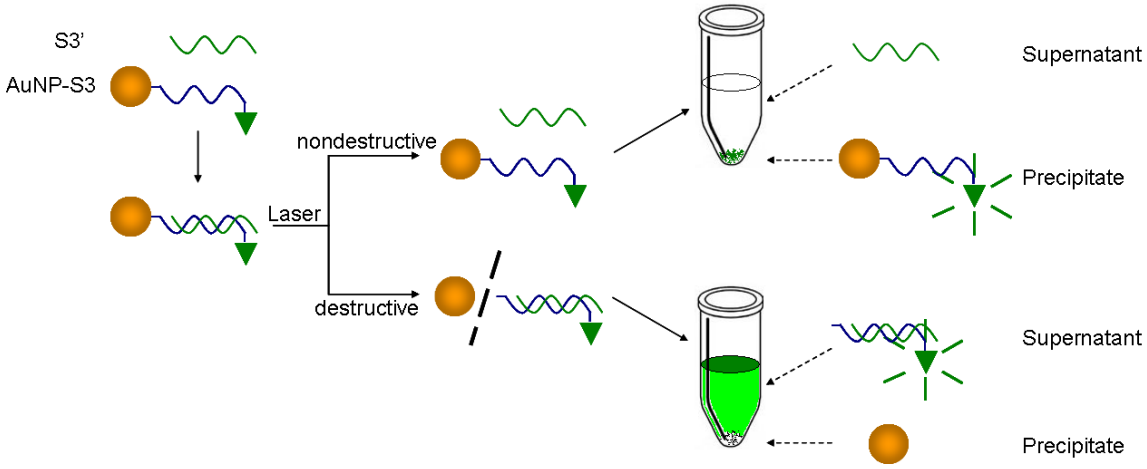

Figure 3.12 Overview of the control experiment. S3 and S3' were hybridized and immobilized on AuNP. Upon irradiation with laser (532 nm, 360 mW, 5 minutes), the solution was centrifuged and the precipitate was re-dispersed. FL intensity of precipitate and supernatant were individually measured to determine whether the fluorophore tethered DNAs released from the AuNP.

This experiment was carried out with the 532-nm laser at 360 mW (higher than the power applied in the selective dehybridization experiment). The initial FL signal was noticeably higher than in the AuNP-D1 experiment in Section 3.2.2, due to the different positioning of the fluorophore in the S3 strand (Fig. 3.13a). For AuNP-D3, as the fluorophore is located further away from the AuNP, the quenching effect decreases, thereby stronger FL is expected. The strong FL signal was intentionally designed to track the location of the S3 DNA strand throughout the laser irradiation and centrifugation[43, 101, 102]. After laser irradiation, the FL intensity increased by 106%. We speculate that it is possibly due to the conformational change of DNA: when laser-irradiated, the DNA oligonucleotide conformation may become more dynamic, thus fluorophore at the other end may be able to generate a higher signal. Similar results have been reported by

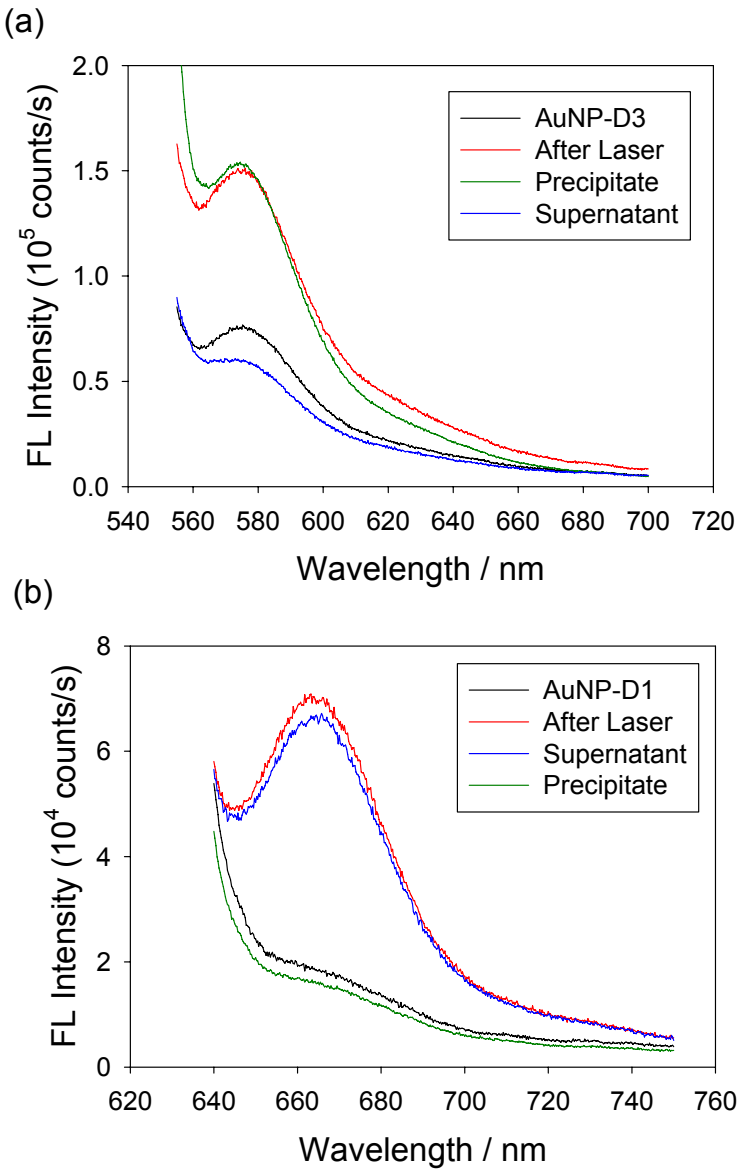

Figure 3.13 (a) AuNP-D3 irradiated by the 532-nm laser at 360 mW for 5 minutes. After laser irradiation, the solution was centrifuged and then precipitate and supernatant were separated (1 trial). (b) AuNP-D1 irradiated by the 532-nm laser at 360 mW for 5 minutes and separated in the same condition (1 trial).

others[103, 104]. Further experiments are required to fully investigate this phenomenon. We focused on the FL change after the precipitate and supernatant were separated. As shown in Fig. 3.13a, the majority of FL (72%) stayed in the precipitate, which convinced us that in this power range the laser

only dehybridizes dsDNA, but does not cleave the S-Au bond. It is noticed that small FL signal (28%) was detected in the supernatant, which may be due to either the non-specifically attached dsDNAs diffusing from the AuNP surface to the solution upon heating (discussed by Sandstrom et al.[103]), or incomplete separation (some AuNP-D3 left in the supernatant, contributing to the FL spectrum).

As a comparison, the same experiment was carried out for AuNP-D1 solution and the result was shown in Fig. 3.13b. When separated after laser irradiation, the majority (80%) of the FL signal is present in the supernatant, while 20% of the FL signal is in the precipitate. The results in Fig. 3.13 demonstrate that after laser irradiation, one ssDNA stays with the AuNP (proven by FL signal in the precipitate in Fig. 3.13a), while the complementary ssDNA is released (proven by FL signal in the supernatant in Fig. 3.13b).

3.3 Selective dehybridization of AuNP-D1 and AuNS-D2 in a mixed solution

In this section, we are going to demonstrate that in a mixed solution of AuNP-D1 and AuNS-D2, each type of DNA-Au nanoconjugates can be dehybridized individually by laser irradiation at its specific wavelength. After both solutions were separately synthesized, 200 μL of 1.1 nM AuNP-D1 was centrifuged and re-dispersed in 200 μL of 1.8 pM AuNS-D2 solution, so that the concentrations of both species in the mixed solution were kept the same. First the solution was subjected to a 299 mW 532-nm laser irradiation for 5 min, and the FL of both Cy5 (represents AuNP-D1) and TAMRA (represents AuNS-D2)

fluorophores were measured before and after irradiation. As shown in Fig. 3.14, the green column represents the Cy5 fluorophore (from AuNP-D1), while the red column represents the TAMRA (from AuNS-D2). The results indicate that the selective dehybridization of AuNP-D1 led to a clear increase in FL intensity and that AuNS-D2 did not respond to 532-nm laser. For AuNP-D1, the Cy5 signal increased to 255±59%, which is in the range of the individual AuNP-D1 solution (248±76%). The TAMRA (from AuNS-D2) signal only increased slightly (8±7%), which is also in the range of the individual AuNS-D2 solution (14±7%). We believe that the heat generated by AuNPs (upon 532-nm laser irradiation) only affects their local environment. In other words, the 532-nm laser can only dehybridize the D1 dsDNA strands attached to the AuNPs, but not the D2 dsDNA strands attached to AuNSs. This is different from the work of Reismann[74], in which the entire solution is heated by the suspended nanostructures.

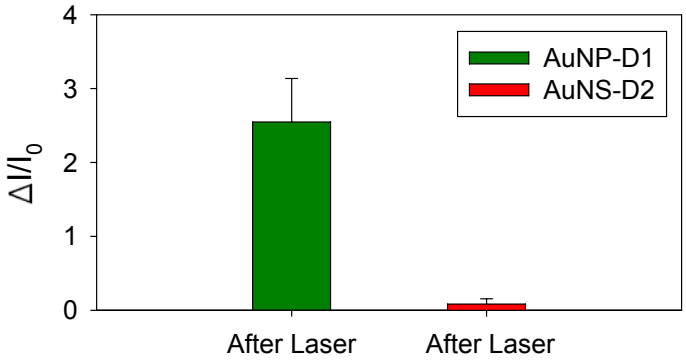

Figure 3.14 532-nm laser induced selective dehybridization of AuNP-D1 in mixed solution at 300 mW for 5 minutes. The error bars represent standard deviation (3 trials).

Fig. 3.15 shows the relative FL intensity changes upon irradiation with 1064-nm laser (244 mW, 5 min). It is clear that the AuNS-D2 (in red) responded to the 1064-nm laser, the TAMRA FL increased by 103±61%; the signal from AuNP-D1 (in green) only increased by 14±10%. These changes are similar to those observed in the individual solutions (Fig. 3.7 and Fig. 3.10). In combination with the results presented in Fig. 3.14, we have demonstrated the selectivity of photothermal heating effect on two different DNA-Au nanoconjugates in a mixed solution. The TEM images of the samples after laser irradiation confirmed the insignificant changes in the AuNP and AuNS morphologies (Fig. 3.16b&c).

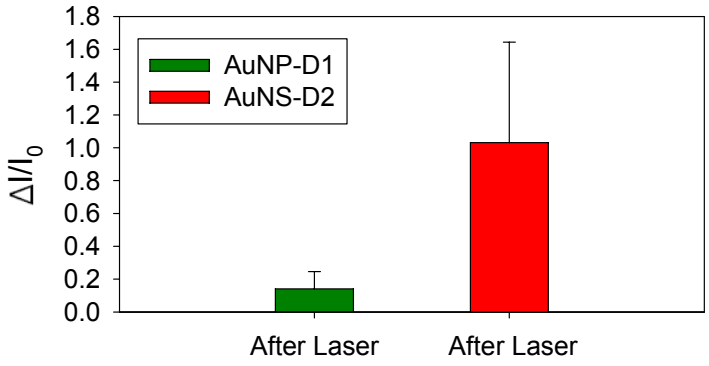

Figure 3.15 1064-nm laser induced selective dehybridization of AuNS-D2 in a mixed solution at 250 mW for 5 minutes. The error bars represent standard deviation (3 trials).

The laser power dependence of the selective dehybridization in a mixed solution was also tested. After laser irradiation, the solution was incubated in a water bath in 80 °C for 5 minutes to conventionally dehybridize all available dsDNAs. Another 5 minutes incubation shows no further FL intensity increase, hence 5 minutes is sufficient for thermal dehybridization. The relative FL intensity

increase of the solution with 532-nm laser irradiation is shown in Fig. 3.16a. The AuNP-D1 signal (in green) showed a clear monotonic increase in FL intensity with increasing 532-nm laser power. After conventional heating, the $\Delta I/I_0$ of AuNP-D1 increased to 3.01, while the $\Delta I/I_0$ of AuNS-D2 increased to 1.41. From the AuNP-D1 result, the amount of S1' dehybridized from AuNP by 299 mW 532-nm laser is 1.87/3.01=62% of the maximum amount of S1' available, thus the laser is proven as a relative capable method to dehybridize dsDNAs. On the contrary, the corresponding percentage of AuNS-D2 is 0.08/1.41=6%, indicating that the S2' DNA can be dehybridized from AuNS by conventional heating, but

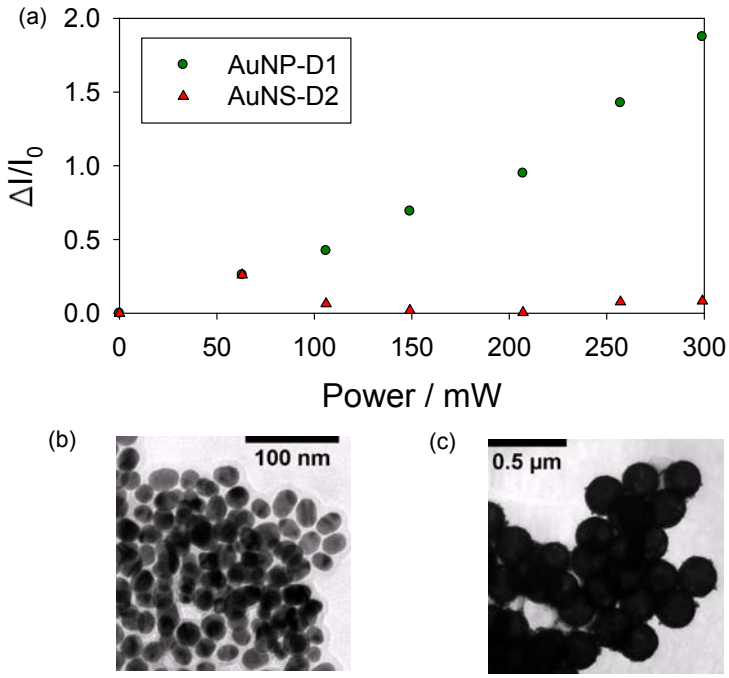

Figure 3.16 A typical example of mixed solution of AuNP-D1 and AuNS-D2 after irradiation by 532-nm laser. (a) Averaged relative FL intensity increase of AuNP-D1 (in green) and AuNS-D2 (in red) as a function of laser power (1 trial). (b) TEM image for AuNP-D1 after conventional heating. (c) TEM image for AuNS-D2 after conventional heating.

not by the 532-nm laser.

The power dependence of the 1064-nm laser is shown in Fig. 3.17. While the AuNS-D2 signal increased monotonically with increasing 1064-nm laser power, the AuNP-D1 signal stayed low. After conventional heating, the $\Delta I/I_0$ of AuNS-D2 increased to 0.98, while the $\Delta I/I_0$ of AuNP-D1 increased to 2.63. The amount of S2' dehybridized from AuNS by 244 mW 1064-nm laser is 0.60/0.98=61% of the maximum amount of S1' available, which indicates high

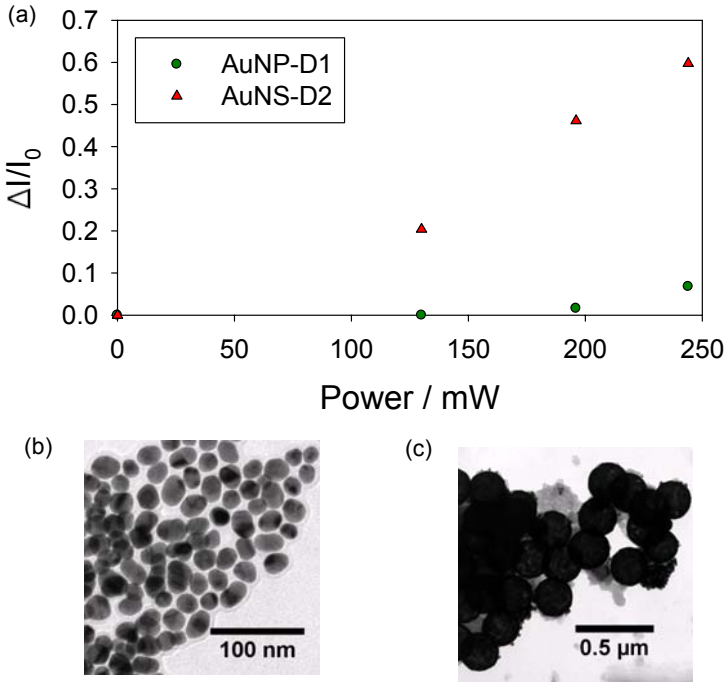

Figure 3.17 A typical example of mixed solution of AuNP-D1 and AuNS-D2 after irradiation by 1064-nm laser. (a) Averaged relative FL intensity increase of AuNP-D1 (in green) and AuNS-D2 (in red) as a function of laser power (1 trial). (b) TEM image for AuNP-D1 after conventional heating. (c) TEM image for AuNS-D2 after conventional heating.

dehybridization percentage by 1064-nm laser irradiation. The corresponding percentage of AuNP-D1 is only 0.07/2.63=3%.

Herein we have shown the selectivity of DNA dehybridization by laser irradiation, particularly in a mixed solution. Laser irradiation at a particular wavelength only heats one specific nanostructure and dehybridizes the attached dsDNA. For example, the 532-nm laser only heats up AuNP and dehybridizes the D1, and vice versa. These results also confirm that the heat generated by one nanostructure does not radiate to the neighbouring nanostructures and corresponding dsDNAs in a mixed solution. In other words, the photothermal effect is confined to the surface of the nanostructure so that only the directly attached dsDNAs are affected.

We believe the selective heating has great potential in various research areas. For instance, a gold nanoparticle can be linked to the end of a DNA hairpin structure. Upon irradiation with the “corresponding” laser, the duplex section will dehybridize and the hairpin will become a “stretched” ssDNA. When laser irradiation stops, the duplex section can reform by rehybridization, because the two corresponding ssDNA sections are in close proximity. As a result, the laser will function as a stimulus to switch “ON” and “OFF” for the hairpin structure. In this way, a hairpin structure can perform as an allosteric regulator (allosteric inhibitor, to be specific) to control the “ON” and “OFF” of more complicated, functional DNA constructs [105-110].

4: CONCLUSION AND FUTURE DIRECTIONS

4.1 Conclusion

In conclusion, this work demonstrates the feasibility of dehybridizing dsDNA attached to the gold nanostructures (nanoparticles and nanoshells) selectively in a mixed solution of AuNP and AuNS by laser irradiation at selected wavelengths. This laser produced SPR heating can be used as a “remote trigger” to release ssDNA strands from gold nanostructures. The irradiation time was investigated to optimize for high dehybridization percentage. It was demonstrated that the percentage of the amount of released DNAs can be controlled by adjusting laser power. Our control experiments with dual-labelled DNA have shown that the laser irradiation does not cause destruction of the bond between thiolated DNA and gold nanostructures.

4.2 Future Directions

4.2.1 Selective release of multiple DNAs from one DNA-nanostructure complex

I believe that this project can be further developed in the hope for more precise and elaborate control of bio-recognition reactions on nanomaterials. I propose that such light-induced dehybridization reactions can be carried out on a single unit, relatively long DNA construct, as illustrated in Fig. 4.1. The target long ssDNA (thin line in Fig. 4.1) can be designed to have three functional regions: R1 (green), R2 (red) and the bridge region (black). Each region can

hybridize with the corresponding complementary sequence (bold lines in Fig. 4.1). R1 can be modified with an AuNP, while R2 can be modified with an AuNS. The goal of this experiment would be to selectively release a piece of DNA strand from either end of the target DNA construct, i.e., to use different laser wavelengths to release the short strands from the two ends. To monitor such reactions, two different fluorophores can be linked to the two ends of the target DNA, so that a specific FL signal would increase when the respective region is activated by laser irradiation. This is a more precise and delicate DNA release mechanism, as both released ssDNAs (R1 and R2) are from the same dsDNA. This would make it possible to manipulate the structures and functions within the same dsDNA structure, so that different input signals (laser irradiations) would achieve different structures and functions.

The most important and delicate part in this design would be the bridge region. As aforementioned, laser irradiation is most effective within the thin layer of water of approximately 5 nm thickness around the nanostructure in aqueous solution[78, 79]. Thus the bridge section should be placed between the two functional end sections so that they are at least 5 nm apart from each other, eliminating the possibility of any interference. The bridge section could be single-stranded but that would make the target DNA flexible, leading towards possible self-folding which can bring the two ends too close. So dsDNA is a superior candidate for the bridge region. We would begin with a 60-base-pair bridge section (20 nm long) to ensure no interference takes place, while each of the two functional sections would be 15 base pairs long. Once individual control on the

two functional sections is achieved, shorter bridge sections should be studied to investigate the minimal length.

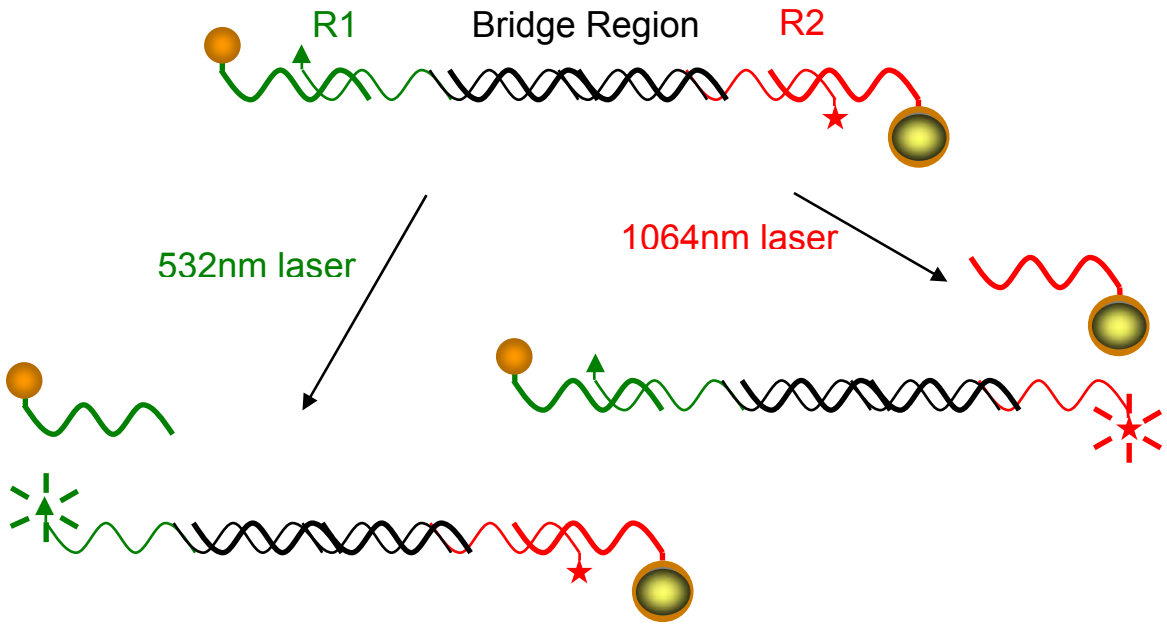

Figure 4.1 Proposed model where different regions within one DNA sequence are activated through dehybridization by different lasers. The target DNA (thin line) is constituted of three regions: R1 (green), R2 (red) and bridge region (black). Each region is hybridized with the respective complementary sequence. R1 is modified with an AuNP, while R2 is modified with an AuNS. Two different fluorophores are linked to the two ends of the target DNA, so that a specific FL signal would increase when the respective region is activated by laser.

Another noteworthy aspect of this design is the positioning of the Au nanostructures and fluorophores. There are two potential positioning combinations. In option one, the target DNA strand can be modified with fluorophores, while the two short strands can be modified with thiols and can be linked to Au nanostructures later on. Option two is to link two thiols to both ends of the target DNA strand and one fluorophore to each short strand. The first option is preferred because it is easy to dual-label target DNA with two different

fluorophores, but difficult to attach two different Au nanostructures specifically on dual labelled thiolated DNA. If both ends of the target DNA strand were modified with thiols, it would be impossible to link two different Au nanostructures to them, as the two thiols have equal probability to link to one Au nanostructure. If the first option is used, dual-labelled fluorophore-DNA can be easily synthesized. Each short strand will contain only one thiol, it can be designated to link to a specific Au nanostructure effortlessly. Once this system is successfully tested, more complicated DNA structures (a double-crossover structure[111, 112], for instance) and other nanoconjugates could be incorporated for a more advanced remote control system.

4.2.2 Activation of aptamer / Au nanoconjugates by laser irradiation

The successful selective DNA dehybridization on AuNP and AuNS induced by laser irradiation opens a great possibility for remote manipulation of DNA-Au nanoconjugates. By immobilizing DNA aptamers on gold nanostructures, we may explore the possibility of fabricating “laser-tuneable” biosensors for small molecules and proteins. Aptamers are nucleic acid (DNA or RNA) receptors that are selected in vitro from large combinatorial pools of sequences to bind specific target molecules such as proteins, organic dyes, or other nucleic acids[113-118]. The goal here is to activate (or turn “ON”) different aptamers by irradiations with lasers at different corresponding wavelengths in a mixed binding solution. In our preliminary experiment, we have replaced the D1 dsDNA with the adenosine aptamer (S4) and its complementary strand (S4’) in the AuNP-D1 nanoconjugate (Fig. 4.2), forming AuNP-D4. The S4 strand is

modified at 5' with a thiol moiety for attaching to AuNP, while 3' is tethered with a fluorophore (Cy5). Since the fluorophore is tethered to the far end of the DNA, low or moderate FL intensity is expected in the beginning. Then the target molecule adenosine (AD) can then be added. Since the aptamer DNA is fully hybridized, the FL intensity should not change. After 532-nm laser irradiation, dsDNA would be dehybridized, exposing the aptamer single strands to bind adenosine. Since the concentration of S4' in solution (diffused out from dsDNA) is expected to be much lower than that of adenosine, also rehybridization is dynamically hindered at room temperature, hence aptamer DNA would bind to adenosine and form a hairpin structure to accommodate two adenosine molecules[81, 82, 118-122] (Fig. 4.3). This conformational change would bring the two ends of the aptamer close to each other, which would inevitably bring AuNP and fluorophore close together, resulting in FL quenching.

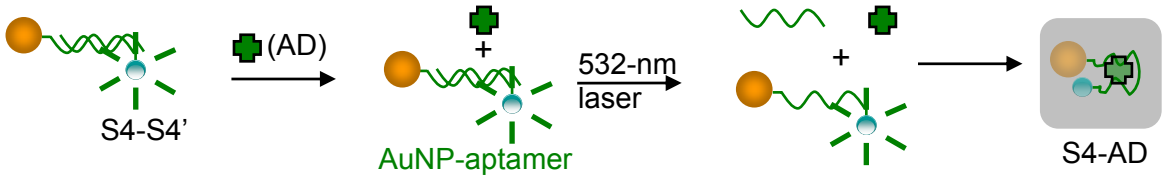

Figure 4.2 Scheme of aptamer activation by laser. Aptamer ssDNA S4 (green) linked at 5' to AuNP, at 3' to a fluorophore. In the initial state S4 prefers to bind to its complementary strand S4'. After dehybridization by laser irradiation, it is supposed to bind to its target adenosine, bringing the fluorophore close to the AuNP and thus decreasing FL intensity.

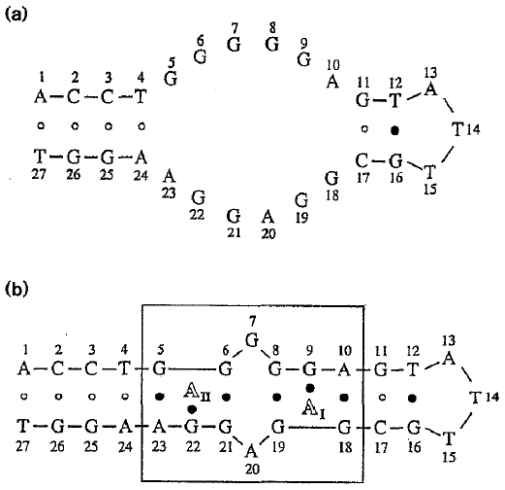

Figure 4.3 Structure of adenosine aptamer. (a) Sequence and Watson-Crick pairing alignments of the adenosine-binding DNA aptamer. (b) Secondary folding structure of the aptamer-adenosine complex, with two non-equivalent binding sites A_I and A_{II}. Dot represents Watson-Crick base pairing, while circle represents wobble base pairing. Adapted from reference 82.

The FL spectra of AuNP-D3 solution trial (named T1) were obtained first as control experiment. In T1 we tried to test whether the aptamer S3 prefers to bind to target AD without the help of laser. When the dsDNA was immobilized on AuNP, the original FL was found to be relatively low (Fig. 3.20). Then the solution was incubated with 1.0 mM AD for 30 min. No significant change in FL intensity was observed. This can be explained that the double-helical interaction (in S3-S3') is much stronger than the aptamer-target interaction (in S3-AD). When the S3 is hybridized, its aptamer function is disabled (turned "OFF").

In another trial (named T2), upon laser irradiation (532-nm laser at 355 mW) for 5 min, we have found that the FL intensity increased significantly. This is an unexpected result since we expected that the FL intensity would decrease as

a result of the folding of adenosine aptamer (which brings the Cy5 closer to the gold surface). After irradiation, the T2 solution was heated to 85 °C and no further fluorescence increase was detected.

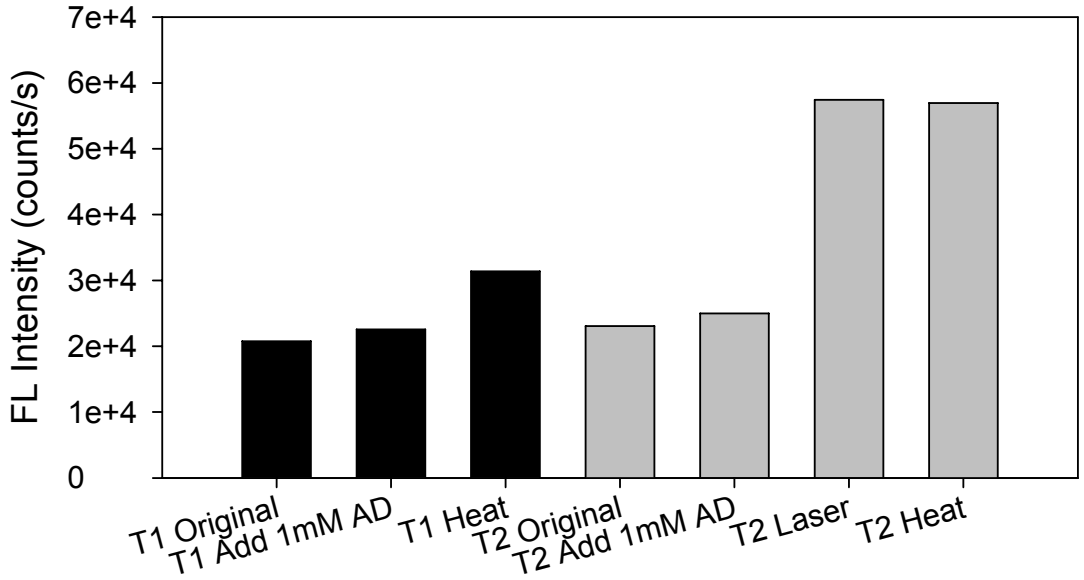

Figure 4.4 Laser triggered aptamer binding experiment. In T1 (black column), dsDNA-AuNP was added with AD first and then heated to 85 °C for 5 minutes. In T2 (gray column), dsDNA-AuNP was added with AD first, followed by laser irradiation, and finally conventional heating.

A possible reason that the aptamer did not bind to adenosine is the relatively small binding constant of aptamer (S3)-adenosine compared with that of the hybridization between S3 and S3'. The aptamer-adenosine complex S3-AD has a dissociation constant of K = 6±3 uM[110-112]. So the standard Gibbs free energy ΔG_m^{θ} for the formation of S3-AD

$$S3 + AD \rightleftharpoons S3\text{-}AD$$

was calculated as ΔG_m^{θ}(S3-AD) = -RTlnK^{-1} = -1.27x10^4 cal/mol. On the other hand, for the hybridization of S3-S3'

$$S3 + S3' \rightleftharpoons S3\text{-}S3'$$

ΔG_m^{θ}(S3-S3') = -5.99 x10^4 cal/mol according to Breslauer's calculation[118]. By comparing the ΔG_m^{θ} values, it is clear that S3 has a high tendency to form S3-S3' dsDNA over the formation of a S3-AD complex.

Besides redesigning the system (e.g., shortening the S3' to a partially complementary strand), we should also check other reaction conditions carefully. For example, the stability of aptamer-adenosine complex is also dependent on the salt concentration. A detailed literature search revealed that 30 mM $MgCl_2$, 100 mM NaCl, and 20 mM Tris-HCl (pH=7.5) were required to form a folded aptamer-adenosine complex on an AuNP surface[116] (Fig. 3.22). The buffer used in this thesis was PBS, which lacks the $MgCl_2$. Although PBS was the universal buffer for general biochemical reactions to take place, Zhao et al.[116] claimed that the dication Mg^{2+} is the key component for the folding of the adenosine aptamer on AuNP surface.

Combining these two designs (4.2.1 and 4.2.2), a long ssDNA hybridized with different short ssDNA aptamers simultaneously may function as a multi-purpose biosensor. The long ssDNA (acts as an inhibitor) may include several regions, each hybridized with a different aptamer as well as a gold nanostructure (nanoparticle, nanoshell or nanorod) with different maximum absorption wavelengths. This solution may be stored in the inactive state, where all the

aptamer strands are present in their hybridized state. Depending on the target of interest, one could activate a certain aptamer by irradiation with a laser of specific wavelength. The active aptamer can then bind to its target, confirming its existence and concentration. Multiple targets can be detected consecutively by programming the laser wavelength. Since a miniaturized laser irradiation module has been developed for nanostructure SPR heating in related research before[102], this system can be integrated into a portable device and programmed such that its operation does not require deep scientific training. We hope that this fundamental research can build the foundation of multi-target detection system that can be applied to a variety of tasks in medical treatment, food safety, pollution control and other areas in the future.

4.2.3 Laser Activation of DNA hairpin/Au Nanoconjugates

Besides aptamer, other nucleic acid hairpin structures can also be incorporated into nanostructure conjugate. Hairpin occurs when two regions of the same strand, usually complementary in nucleotide sequence, base-pair to form a double helix that ends in an unpaired loop[123, 124]. They are important model systems for studying the conformational dynamics of nucleic acid biopolymers, as well as for understanding the primary mechanism of complimentary DNA or RNA duplex formation[125]. The hairpin-forming RNA and DNA structures have important regulatory roles in cellular metabolism[126, 127], so the success in manipulation of their conformation could lead to remote control of corresponding process or mechanism. For example, silencing RNAs interact with members of the Argonaute family of proteins, which they guide to their regulatory

targets, typically resulting in reduced expression of target genes[128]. If the RNA is modified with an AuNP on one end and a fluorophore on the other end, then the presence of FL signal would indicate the hybridization/dehybridization status of the RNA strand. When the laser irradiation is off, the RNA hairpin structure forms thus can be recognized by the protein and regulates. When laser irradiates, the RNA dehybridizes, so that its interaction with the protein is hindered. By doing so, the regulatory functions of different RNAs can be remotely controlled by laser irradiation. This work would greatly contribute to the investigation in mechanism of target regulation by RNAs. However, it is noteworthy that this remote control is effective only when a conformation change can be triggered by local heating. Also the nanostructure (needs to present in the stem region of the hairpin) must not interfere with the target regulation. If a long stem region needs to dehybridize, more than one nanostructure can be linked to homogeneously heat and dehybridize the double strand. On a related research, the RNA sequence can be replaced by DNA sequence, for example, adenosine aptamer used in section 4.2.2. By doing so, the conformational change of a ssDNA aptamer (without presence of target) on AuNP surface upon heating can be studied. As a comparison to the research in section 4.2.2, this would provide valuable information about the mechanism of the interaction between aptamer and target on AuNP surface.

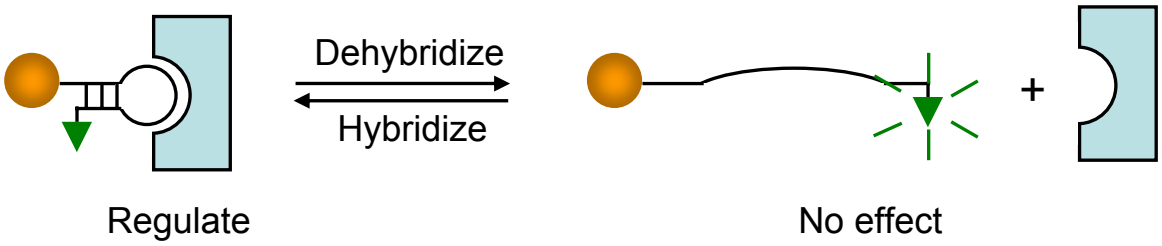

Figure 4.5 Conformational change of a DNA hairpin controlled by laser irradiation induced dehybridization. The blue object represents protein.

REFERENCE LIST

1. Wagner, F. E.; Haslbeck, S.; Stievano, L.; Calogero, S.; Pankhurst, Q. A.; Martinek, P., Before striking gold in gold-ruby glass. *Nature* **2000,** 407, (6805), 691-692.

2. Daniel, M., Gold nanoparticles: Assembly, supramolecular chemistry, quantum-size-related properties, and applications toward biology, catalysis, and nanotechnology. *Chem. Rev.* **2004,** 104, (1), 293-346.

3. Leonhardt, U., Optical metamaterials - Invisibility cup. *Nat. Photonics* **2007,** 1, (4), 207-208.

4. Ostwald, W., Zur Geschichte des Colloiden Goldes. *Kolloid Z.* **1909,** 4, 5.

5. Faraday, M., The Bakerian Lecture: Experimental Relations of Gold (and Other Metals) to Light. *Philos. Trans. R. Soc. London* **1857,** 147, 145-181.

6. Levin, C. S.; Kundu, J.; Barhoumi, A.; Halas, N. J., Nanoshell-based substrates for surface enhanced spectroscopic detection of biomolecules. *Analyst* **2009,** 134, (9), 1745-1750.

7. Fischler, M.; Simon, U., Metal nanoparticle-DNA hybrids - from assembly towards functional conjugates. *J. Mater. Chem.* **2009,** 19, (11), 1518-1523.

8. Perez-Juste, J.; Pastoriza-Santos, I.; Liz-Marzan, L. M.; Mulvaney, P., Gold nanorods: Synthesis, characterization and applications. In 2005; pp 1870-1901.

9. Loo, C.; Lin, A.; Hirsch, L.; Lee, M. H.; Barton, J.; Halas, N.; West, J.; Drezek, R., Nanoshell-enabled photonics-based imaging and therapy of cancer. *Technol. Cancer Res. T.* **2004,** 3, (1), 33-40.

10. Dulkeith, E.; Morteani, A. C.; Niedereichholz, T.; Klar, T. A.; Feldmann, J.; Levi, S. A.; van Veggel, F.; Reinhoudt, D. N.; Moller, M.; Gittins, D. I., Fluorescence quenching of dye molecules near gold nanoparticles: Radiative and nonradiative effects. *Phys. Rev. Lett.* **2002,** 89, (20), 1-4.

11. Turkevich, J.; Stevenson, P. C.; Hillier, J., A Study of the Nucleation and Growth Processes in the Synthesis of Colloidal Gold. *Discuss. Faraday. Soc.* **1951**, (11), 55-75.

12. Kimling, J.; Maier, M.; Okenve, B.; Kotaidis, V.; Ballot, H.; Plech, A., Turkevich method for gold nanoparticle synthesis revisited. *J. Phys. Chem. B* **2006,** 110, (32), 15700-15707.

13. Frens, G., Controlled Nucleation for Regulation of Particle-Size in Monodisperse Gold Suspensions. *Nature-Physical Science* **1973,** 241, (105), 20-22.

14. Kuyper, A. C., The oxidation of citric acid. *Journal of the American Chemical Society* **1933,** 55, 1722-1727.

15. Cardenas, M.; Barauskas, J.; Schillen, K.; Brennan, J. L.; Brust, M.; Nylander, T., Thiol-speciric and nonspecific interactions between DNA and gold nanoparticles. *Langmuir* **2006,** 22, (7), 3294-3299.

16. Link, S.; El-Sayed, M. A., Size and Temperature Dependence of the Plasmon Absorption of Colloidal Gold Nanoparticles. *J. Phys. Chem. B* **1999,** 103, (21), 4212-4217.

17. Jain, P. K.; Lee, K. S.; El-Sayed, I. H.; El-Sayed, M. A., Calculated absorption and scattering properties of gold nanoparticles of different size, shape, and composition: Applications in biological imaging and biomedicine. *J. Phys. Chem. B* **2006,** 110, (14), 7238-7248.

18. Haiss, W.; Thanh, N. T. K.; Aveyard, J.; Fernig, D. G., Determination of size and concentration of gold nanoparticles from UV-Vis spectra. *Anal. Chem.* **2007,** 79, (11), 4215-4221.

19. Mie, G., Articles on the optical characteristics of turbid tubes, especially colloidal metal solutions. *Annalen Der Physik* **1908,** 25, (3), 377-445.

20. Kelly, K. L.; Coronado, E.; Zhao, L. L.; Schatz, G. C., The optical properties of metal nanoparticles: The influence of size, shape, and dielectric environment. *J. Phys. Chem. B* **2003,** 107, (3), 668-677.

21. Busbee, B. D.; Obare, S. O.; Murphy, C. J., An improved synthesis of high-aspect-ratio gold nanorods. *Adv. Mater.* **2003,** 15, (5), 414-416.

22. Wijaya, A.; Schaffer, S. B.; Pallares, I. G.; Hamad-Schifferli, K., Selective Release of Multiple DNA Oligonucleotides from Gold Nanorods. *ACS Nano* **2009,** 3, (1), 80-86.

23. Averitt, R. D.; Westcott, S. L.; Halas, N. J., Linear optical properties of gold nanoshells. *J. Opt. Soc. Am. B* **1999,** 16, (10), 1824-1832.

24. Oldenburg, S. J.; Averitt, R. D.; Westcott, S. L.; Halas, N. J., Nanoengineering of optical resonances. *Chem. Phys. Lett.* **1998,** 288, (2-4), 243-247.

25. Hirsch, L. R.; Gobin, A. M.; Lowery, A. R.; Tam, F.; Drezek, R. A.; Halas, N. J.; West, J. L., Metal nanoshells. *Ann. Biomed. Eng.* **2006,** 34, (1), 15-22.

26. Kalele, S.; Gosavi, S. W.; Urban, J.; Kulkarni, S. K., Nanoshell particles: synthesis, properties and applications. *Curr. Sci.* **2006,** 91, (8), 1038-1052.

27. Loo, C.; Lowery, A.; Halas, N.; West, J.; Drezek, R., Immunotargeted nanoshells for integrated cancer imaging and therapy. *Nano Lett.* **2005,** 5, (4), 709-711.

28. Sokolov, K.; Follen, M.; Aaron, J.; Pavlova, I.; Malpica, A.; Lotan, R.; Richards-Kortum, R., Real-time vital optical imaging of precancer using anti-epidermal growth factor receptor antibodies conjugated to gold nanoparticles. *Cancer Research* **2003,** 63, (9), 1999-2004.

29. Wang, Y.; Qian, W. P.; Tan, Y.; Ding, S. H., A label-free biosensor based on gold nanoshell monolayers for monitoring biomolecular interactions in diluted whole blood. *Biosens. Bioelectron.* **2008,** 23, (7), 1166-1170.

30. Malinsky, M. D.; Kelly, K. L.; Schatz, G. C.; Van Duyne, R. P., Chain length dependence and sensing capabilities of the localized surface plasmon resonance of silver nanoparticles chemically modified with alkanethiol self-assembled monolayers. *J. Am. Chem. Soc.* **2001,** 123, (7), 1471-1482.

31. Nath, N.; Chilkoti, A., A colorimetric gold nanoparticle sensor to interrogate biomolecular interactions in real time on a surface. *Anal. Chem.* **2002,** 74, (3), 504-509.

32. Haes, A. J.; Chang, L.; Klein, W. L.; Van Duyne, R. P., Detection of a biomarker for Alzheimer's disease from synthetic and clinical samples using a nanoscale optical biosensor. *J. Am. Chem. Soc.* **2005,** 127, (7), 2264-2271.

33. Nath, N.; Chilkoti, A., A colorimetric gold nanoparticle sensor to interrogate biomolecular interactions in real time on a surface. *Analytical Chemistry* **2002,** 74, (3), 504-509.

34. Alivisatos, A. P.; Johnsson, K. P.; Peng, X. G.; Wilson, T. E.; Loweth, C. J.; Bruchez, M. P.; Schultz, P. G., Organization of 'nanocrystal molecules' using DNA. *Nature* **1996,** 382, (6592), 609-611.

35. Mirkin, C. A.; Letsinger, R. L.; Mucic, R. C.; Storhoff, J. J., A DNA-based method for rationally assembling nanoparticles into macroscopic materials. *Nature* **1996,** 382, (6592), 607-609.

36. Mucic, R. C.; Storhoff, J. J.; Mirkin, C. A.; Letsinger, R. L., DNA-directed synthesis of binary nanoparticle network materials. *J. Am. Chem. Soc.* **1998,** 120, (48), 12674-12675.

37. Mirkin, C. A., Programming the assembly of two- and three-dimensional architectures with DNA and nanoscale inorganic building blocks. In Am. Chem. Soc.: 2000; pp 2258-2272.

38. Hurst, S. J.; Lytton-Jean, A. K. R.; Mirkin, C. A., Maximizing DNA loading on a range of gold nanoparticle sizes. *Anal. Chem.* **2006,** 78, (24), 8313-8318.

39. Park, S. Y.; Lytton-Jean, A. K. R.; Lee, B.; Weigand, S.; Schatz, G. C.; Mirkin, C. A., DNA-programmable nanoparticle crystallization. *Nature* **2008,** 451, (7178), 553-556.

40. Hill, H. D.; Macfarlane, R. J.; Senesi, A. J.; Lee, B.; Park, S. Y.; Mirkin, C. A., Controlling the lattice parameters of gold nanoparticle FCC crystals with duplex DNA linkers. *Nano Lett.* **2008,** 8, (8), 2341-2344.

41. Li, H.; Liang, R.; Turner, D. H.; Rothberg, L. J.; Duan, S., Selective quenching of fluorescence from unbound oligonucleotides by gold nanoparticles as a probe of RNA structure. *RNA* **2007,** 13, 2034-2041.

42. Ray, P. C.; Fortner, A.; Griffin, J.; Kim, C. K.; Singh, J. P.; Yu, H. T., Laser-induced fluorescence quenching of tagged oligonucleotide probes by gold nanoparticles. *Chem. Phys. Lett.* **2005,** 414, (4-6), 259-264.

43. Dulkeith, E.; Ringler, M.; Klar, T. A.; Feldmann, J.; Javier, A. M.; Parak, W. J., Gold nanoparticles quench fluorescence by phase induced radiative rate suppression. *Nano Lett.* **2005,** 5, (4), 585-589.

44. Li, H. X.; Rothberg, L. J., DNA sequence detection using selective fluorescence quenching of tagged oligonucleotide probes by gold nanoparticles. *Anal. Chem.* **2004,** 76, (18), 5414-5417.

45. Aslan, K.; Perez-Luna, V. H., Quenched emission of fluorescence by ligand functionalized gold nanoparticles. *J. Fluoresc.* **2004,** 14, (4), 401-405.

46. Dubertret, B.; Calame, M.; Libchaber, A. J., Single-mismatch detection using gold-quenched fluorescent oligonucleotides. *Nat. Biotechnol.* **2001,** 19, (4), 365-370.

47. Weiss, S., Fluorescence spectroscopy of single biomolecules. *Science* **1999,** 283, (5408), 1676-1683.

48. Avouris, P.; Persson, B. N. J., Excited states at metal surfaces and their non-radiative relaxation. *J. Phys. Chem.* **1984,** 88, (5), 837-848.

49. Persson, B. N. J.; Andersson, S., Dynamical processes at surfaces: Excitation of electron-hole pairs. *Phys. Rev. B* **1984,** 29, (8), 4382-4394.

50. Cnossen, G.; Drabe, K. E.; Wiersma, D. A., Fluorescence properties of submonolayers of rhodamine 6G in front of a mirror. *J. Chem. Phys.* **1993,** 98, (7), 5276-5280.

51. Lakowicz, J. R., Radiative decay engineering: Biophysical and biomedical applications. *Anal. Biochem.* **2001,** 298, (1), 1-24.

52. Sokolov, K.; Chumanov, G.; Cotton, T. M., Enhancement of molecular fluorescence near the surface of colloidal metal films. *Anal. Chem.* **1998,** 70, (18), 3898-3905.

53. Liebermann, T.; Knoll, W., Surface-plasmon field-enhanced fluorescence spectroscopy. *Colloids Surf., A* **2000,** 171, (1-3), 115-130.

54. Gryczynski, I.; Malicka, J.; Shen, Y. B.; Gryczynski, Z.; Lakowicz, J. R., Multiphoton excitation of fluorescence near metallic particles: Enhanced and localized excitation. *J. Phys. Chem. B* **2002,** 106, (9), 2191-2195.

55. Hutter, E.; Fendler, J. H., Exploitation of localized surface plasmon resonance. *Adv. Mater.* **2004,** 16, (19), 1685-1706.

56. Homola, J., *Surface Plasmon Resonance Based Sensors*. Berlin: Springer-Verlag: 2006; Vol. 4.

57. Liu, X. O.; Atwater, M.; Wang, J. H.; Huo, Q., Extinction coefficient of gold nanoparticles with different sizes and different capping ligands. *Colloids Surf., B* **2007,** 58, (1), 3-7.

58. Jain, P. K.; Huang, X.; El-Sayed, I. H.; El-Sayad, M. A., Review of some interesting surface plasmon resonance-enhanced properties of noble metal nanoparticles and their applications to biosystems. *Plasmonics* **2007,** 2, (3), 107-118.

59. Perner, M.; Bost, P.; Lemmer, U.; vonPlessen, G.; Feldmann, J.; Becker, U.; Mennig, M.; Schmitt, M.; Schmidt, H., Optically induced damping of the surface plasmon resonance in gold colloids. *Phys. Rev. Lett.* **1997,** 78, (11), 2192-2195.

60. Roper, D. K.; Ahn, W.; Hoepfner, M., Microscale Heat Transfer Transduced by Surface Plasmon Resonant Gold Nanoparticles. *The Journal of Physical Chemistry C* **2007,** 111, (9), 3636-3641.

61. Link, S.; El-Sayed, M. A., Spectral properties and relaxation dynamics of surface plasmon electronic oscillations in gold and silver nanodots and nanorods. *Journal of Physical Chemistry B* **1999,** 103, (40), 8410-8426.

62. El-Sayed, M. A., Some interesting properties of metals confined in time and nanometer space of different shapes. *Accounts of Chemical Research* **2001,** 34, (4), 257-264.

63. Alvarez, M. M.; Khoury, J. T.; Schaaff, T. G.; Shafigullin, M. N.; Vezmar, I.; Whetten, R. L., Optical absorption spectra of nanocrystal gold molecules. *J. Phys. Chem. B* **1997,** 101, (19), 3706-3712.

64. Villringer, A.; Chance, B., Non-invasive optical spectroscopy and imaging of human brain function. *Trends in Neurosciences* **1997,** 20, (10), 435-442.

65. Oldenburg, S. J.; Jackson, J. B.; Westcott, S. L.; Halas, N. J., Infrared extinction properties of gold nanoshells. *Appl. Phys. Lett.* **1999,** 75, (19), 2897-2899.

66. Sershen, S. R.; Westcott, S. L.; Halas, N. J.; West, J. L., Temperature-sensitive polymer-nanoshell composites for photothermally modulated drug delivery. *J. Biomed. Mater. Res.* **2000,** 51, (3), 293-298.

67. Sershen, S. R.; Westcott, S. L.; Halas, N. J.; West, J. L., Independent optically addressable nanoparticle-polymer optomechanical composites. *Appl. Phys. Lett.* **2002,** 80, (24), 4609-4611.

68. Sershen, S. R.; Mensing, G. A.; Ng, M.; Halas, N. J.; Beebe, D. J.; West, J. L., Independent optical control of microfluidic valves formed from optomechanically responsive nanocomposite hydrogels. *Adv. Mater.* **2005,** 17, (11), 1366-1368.

69. Hamad-Schifferli, K.; Schwartz, J. J.; Santos, A. T.; Zhang, S. G.; Jacobson, J. M., Remote electronic control of DNA hybridization through

inductive coupling to an attached metal nanocrystal antenna. *Nature* **2002,** 415, (6868), 152-155.

70. Dillenback, L. M.; Goodrich, G. P.; Keating, C. D., Temperature-programmed assembly of DNA : Au nanoparticle bioconjugates. *Nano Lett.* **2006,** 6, (1), 16-23.

71. Harris, N.; Ford, M. J.; Cortie, M. B., Optimization of plasmonic heating by gold nanospheres and nanoshells. *J. Phys. Chem. B* **2006,** 110, (22), 10701-10707.

72. Jain, P. K.; Qian, W.; El-Sayed, M. A., Ultrafast cooling of photoexcited electrons in gold nanoparticle-thiolated DNA conjugates involves the dissociation of the gold-thiol bond. *J. Am. Chem. Soc.* **2006,** 128, (7), 2426-2433.

73. Stehr, J.; Hrelescu, C.; Sperling, R. A.; Raschke, G.; Wunderlich, M.; Nichtl, A.; Heindl, D.; Kurzinger, K.; Parak, W. J.; Klar, T. A.; Feldmann, J., Gold NanoStoves for microsecond DNA melting analysis. *Nano Lett.* **2008,** 8, (2), 619-623.

74. Reismann, M.; Bretschneider, J. C.; von Plessen, G.; Simon, U., Reversible photothermal melting of DNA in DNA-gold-nanoparticle networks. *Small* **2008,** 4, (5), 607-610.

75. Cantor, C. R.; Schimmel, P., *Biophysical Chemistry*. Freeman: San Francisco, 1980.

76. Rafi, A. A.; Wheeler, C. M., Radiation-Induced Hyperchromicity of DNA. *International Journal of Radiation Biology* **1973,** 24, (3), 321-323.

77. Bonnet, G.; Krichevsky, O.; Libchaber, A., Kinetics of conformational fluctuations in DNA hairpin-loops. *Proc. Natl. Acad. Sci. U. S. A.* **1998,** 95, (15), 8602-8606.

78. Pitsillides, C. M.; Joe, E. K.; Wei, X. B.; Anderson, R. R.; Lin, C. P., Selective cell targeting with light-absorbing microparticles and nanoparticles. *Biophys. J.* **2003,** 84, (6), 4023-4032.

79. Govorov, A. O.; Zhang, W.; Skeini, T.; Richardson, H.; Lee, J.; Kotov, N. A., Gold nanoparticle ensembles as heaters and actuators: melting and collective plasmon resonances. *Nanoscale Res. Lett.* **2006,** 1, (1), 84-90.

80. Cao, Y. W. C.; Jin, R. C.; Mirkin, C. A., Nanoparticles with Raman spectroscopic fingerprints for DNA and RNA detection. *Science* **2002,** 297, (5586), 1536-1540.

81. Huizenga, D. E.; Szostak, J. W., A DNA aptamer that binds adenosine and ATP. *Biochemistry* **1995,** 34, (2), 656-665.

82. Lin, C. H.; Patel, D. J., Structural basis of DNA folding and recognition in an AMP-DNA aptamer complex: distinct architectures but common recognition motifs for DNA and RNA aptamers complexed to AMP. *Chem. Biol.* **1997,** 4, (11), 817-832.

83. Yao, H.; Yi, C. Q.; Tzang, C. H.; Zhu, J. J.; Yang, M. S., DNA-directed self-assembly of gold nanoparticles into binary and ternary nanostructures. *Nanotechnology* **2007,** 18, (1), -.

84. Han, J. C.; Han, G. Y., A Procedure for Quantitative-Determination of Tris(2-Carboxyethyl)Phosphine, an Odorless Reducing Agent More Stable and Effective Than Dithiothreitol. *Anal. Biochem.* **1994,** 220, (1), 5-10.

85. Rüegg, U. T.; Rudinger, J., Reductive cleavage of cystine disulfides with tributylphosphine. In *Methods. Enzymol.*, Academic Press: 1977; Vol. Volume 47, pp 111-116.

86. Rosi, N. L.; Giljohann, D. A.; Thaxton, C. S.; Lytton-Jean, A. K. R.; Han, M. S.; Mirkin, C. A., Oligonucleotide-modified gold nanoparticles for intracellular gene regulation. *Science* **2006,** 312, (5776), 1027-1030.

87. Liang, Z. Q.; Zhang, J.; Wang, L. H.; Song, S. P.; Fan, C. H.; Li, G. X., A centrifugation-based method for preparation of gold nanoparticles and its application in biodetection. *Int. J. Mol. Sci.* **2007,** 8, (6), 526-532.

88. Koechner, W., *Solid-State Laser Engineering*. 6 ed.; Springer: Berlin, 2006.

89. Aboites, V.; Martinez, F.; Jimenez, M., Laser amplification: experiment and electronic simulation. *Revista Mexicana De Fisica E* **2007,** 53, (2), 168-173.

90. Campagnola, P. J.; Mohler, W. H.; Plotnikov, S.; Millard, A. C., Second harmonic generation imaging of endogenous structural proteins. In *Multiphoton Microscopy in the Biomedical Sciences Iii*, Periasamy, A.; So, P. T. C., Eds. 2003; Vol. 4963, pp 73-80.

91. Brown, D. J.; Morishige, N.; Neekhra, A.; Minckler, D. S.; Jester, J. V., Application of second harmonic imaging microscopy to assess structural changes in optic nerve head structure ex vivo. *Journal of Biomedical Optics* **2007,** 12, (2).

92. Powerlite Precision II 8000. http://www.continuumlasers.com/products/pdfs/Powerlite_Prec_II_8000.pdf

93. Shuford, K. L.; Ratner, M. A.; Schatz, G. C., Multipolar excitation in triangular nanoprisms. *J. Chem. Phys.* **2005,** 123, (11).

94. Wu, D. J.; Xu, X. D.; Liu, X. J., Influence of dielectric core, embedding medium and size on the optical properties of gold nanoshells. *Solid State Commun.* **2008,** 146, (1-2), 7-11.

95. Liu, G. L.; Yin, Y. D.; Kunchakarra, S.; Mukherjee, B.; Gerion, D.; Jett, S. D.; Bear, D. G.; Gray, J. W.; Alivisatos, A. P.; Lee, L. P.; Chen, F. Q. F., A nanoplasmonic molecular ruler for measuring nuclease activity and DNA footprinting. *Nature Nanotechnology* **2006,** 1, (1), 47-52.

96. Bakhtiari, A. B. S.; Hsiao, D.; Jin, G.; Gates, B. D.; Branda, N. R., An Efficient Method Based on the Photothermal Effect for the Release of Molecules from Metal Nanoparticle Surfaces. *Angew. Chem.* **2009,** 48, (23), 4166-4169.

97. Wetmur, J. G., DNA PROBES - APPLICATIONS OF THE PRINCIPLES OF NUCLEIC-ACID HYBRIDIZATION. *Critical Reviews in Biochemistry and Molecular Biology* **1991,** 26, (3-4), 227-259.

98. Schelm, S.; Smith, G. B., Evaluation of the limits of resonance tunability in metallic nanoshells with a spectral averaging method. *Journal of the Optical Society of America a-Optics Image Science and Vision* **2005,** 22, (7), 1288-1292.

99. Hleb, E. Y.; Lapotko, D. O., Photothermal properties of gold nanoparticles under exposure to high optical energies. *Nanotechnology* **2008,** 19, (35).

100. Herdt, A. R.; Drawz, S. M.; Kang, Y. J.; Taton, T. A., DNA dissociation and degradation at gold nanoparticle surfaces. *Colloids Surf., B* **2006,** 51, (2), 130-139.

101. Ray, P. C.; Darbha, G. K.; Ray, A.; Hardy, W.; Walker, J., A gold-nanoparticle-based fluorescence resonance energy transfer probe for multiplexed hybridization detection: accurate identification of bio-agents DNA. *Nanotechnology* **2007,** 18, (37).

102. Kim, C. K.; Kalluru, R. R.; Singh, J. P.; Fortner, A.; Griffin, J.; Darbha, G. K.; Ray, P. C., Gold-nanoparticle-based miniaturized laser-induced fluorescence probe for specific DNA hybridization detection: studies on size-dependent optical properties. *Nanotechnology* **2006,** 17, (13), 3085-3093.

103. Sandstrom, P.; Boncheva, M.; Akerman, B., Nonspecific and thiol-specific binding of DNA to gold nanoparticles. *Langmuir* **2003,** 19, (18), 7537-7543.

104. Park, S.; Brown, K. A.; Hamad-Schifferli, K., Changes in oligonucleotide conformation on nanoparticle surfaces by modification with mercaptohexanol. *Nano Letters* **2004,** 4, (10), 1925-1929.

105. Soukup, G. A.; Breaker, R. R., Design of allosteric hammerhead ribozymes activated by ligand-induced structure stabilization. *Structure with Folding & Design* **1999,** 7, (7), 783-791.

106. Soukup, G. A.; Breaker, R. R., Engineering precision RNA molecular switches. *Proceedings of the National Academy of Sciences of the United States of America* **1999,** 96, (7), 3584-3589.

107. Soukup, G. A.; Breaker, R. R., Nucleic acid molecular switches. *Trends in Biotechnology* **1999,** 17, (12), 469-476.

108. Soukup, G. A.; Breaker, R. R., Allosteric nucleic acid catalysts. *Current Opinion in Structural Biology* **2000,** 10, (3), 318-325.

109. Soukup, G. A.; Emilsson, G. A. M.; Breaker, R. R., Altering molecular recognition of RNA aptamers by allosteric selection. *Journal of Molecular Biology* **2000,** 298, (4), 623-632.

110. Cong, X. Y.; Nilsen-Hamilton, M., Allosteric aptamers: Targeted reversibly attenuated probes. *Biochemistry* **2005,** 44, (22), 7945-7954.

111. Li, X. J.; Yang, X. P.; Qi, J.; Seeman, N. C., Antiparallel DNA double crossover molecules as components for nanoconstruction. *Journal of the American Chemical Society* **1996,** 118, (26), 6131-6140.

112. Shih, W. M.; Quispe, J. D.; Joyce, G. F., A 1.7-kilobase single-stranded DNA that folds into a nanoscale octahedron. *Nature* **2004,** 427, (6975), 618-621.

113. Cheng, A. K. H.; Ge, B.; Yu, H. Z., Aptamer-based biosensors for label-free voltammetric detection of lysozyme. *Analytical Chemistry* **2007,** 79, (14), 5158-5164.

114. Tuerk, C.; Gold, L., Systematic evolution of ligands by exponential enrichment: RNA ligands to bacteriophage T4 DNA polymerase. *Science* **1990,** 249, (4968), 505-510.

115. Ellington, A. D.; Szostak, J. W., INVITRO SELECTION OF RNA MOLECULES THAT BIND SPECIFIC LIGANDS. *Nature* **1990,** 346, (6287), 818-822.

116. Gold, L.; Polisky, B.; Uhlenbeck, O.; Yarus, M., Diversity of oligonucleotide functions. *Annu. Rev. Biochem.* **1995,** 64, 763-797.

117. Chakraborty, B.; Jiang, Z.; Li, Y.; Yu, H.-Z., Rational design and performance testing of aptamer-based electrochemical biosensors for adenosine. *J. Electroanal. Chem.* **2009,** 635, (2), 75-82.

118. Fahlman, R. P.; Sharma, R. D.; Sen, D., The Charge Conduction Properties of DNA Holliday Junctions Depend Critically on the Identity of the Tethered Photooxidant. *J. Am. Chem. Soc.* **2002,** 124, (42), 12477-12485.

119. Zhao, W. A.; Chiuman, W.; Brook, M. A.; Li, Y. F., Simple and rapid colorimetric biosensors based on DNA aptamer and noncrosslinking gold nanoparticle aggregation. *ChemBioChem* **2007,** 8, (7), 727-731.

120. Zuo, X. L.; Song, S. P.; Zhang, J.; Pan, D.; Wang, L. H.; Fan, C. H., A target-responsive electrochemical aptamer switch (TREAS) for reagentless detection of nanomolar ATP. *J. Am. Chem. Soc.* **2007,** 129, 1042-1043.

121. Zhao, W. A.; Chiuman, W.; Lam, J. C. F.; McManus, S. A.; Chen, W.; Cui, Y. G.; Pelton, R.; Brook, M. A.; Li, Y. F., DNA aptamer folding on gold nanoparticies: From colloid chemistry to biosensors. *J. Am. Chem. Soc.* **2008,** 130, (11), 3610-3618.

122. Li, F.; Zhang, J.; Cao, X. N.; Wang, L. H.; Li, D.; Song, S. P.; Ye, B. C.; Fan, C. H., Adenosine detection by using gold nanoparticles and designed aptamer sequences. *Analyst* **2009,** 134, (7), 1355-1360.

123. Watson, J. D.; Baker, T. A.; Bell, S. P.; Gann, A.; Levine, M.; Losick, R., *Molecular Biology of the Gene*. 5th ed.; Cold Spring Harbor Laboratory Press: 2003.

124. Varani, G., EXCEPTIONALLY STABLE NUCLEIC-ACID HAIRPINS. *Annual Review of Biophysics and Biomolecular Structure* **1995,** 24, 379-404.

125. Van Orden, A.; Jung, J., Fluorescence correlation spectroscopy for probing the kinetics and mechanisms of DNA hairpin formation. *Biopolymers* **2008,** 89, (1), 1-16.

126. Cech, T. R., CATALYTIC RNA - STRUCTURE AND MECHANISM. *Biochemical Society Transactions* **1993,** 21, (2), 229-234.

127. Pearson, C. E.; Sinden, R. R., Trinucleotide repeat DNA structures: dynamic mutations from dynamic DNA. *Current Opinion in Structural Biology* **1998,** 8, (3), 321-330.

128. Ghildiyal, M.; Zamore, P. D., Small silencing RNAs: an expanding universe. *Nature Reviews Genetics* **2009,** 10, (2), 94-108.